# On the relationship between the water mass pathways and eddy variability in the Western Mediterranean Sea

E.K. Demirov

Department of Physics and Physical Oceanography, Memorial University of Newfoundland, St. John's, NL, Canada

N. Pinardi

Bologna University, Corso di Scienze Ambientali, Ravenna, Italy

Istituto Nazionale di Geofisica e Vulcanologia, Bologna, Italy

E. K. Demirov, Department of Physics and Physical Oceanography, Memorial University of Newfoundland, St. John's, NL, A1B 3X7, Canada (entcho@physics.mun.ca)

**Abstract.**

The role of eddies on the formation and spreading of water masses in the Western Mediterranean Sea is studied with an ocean general circulation model. The model is forced with interannually variable surface forcing for the years from 1979 to 1999. It is found that the model reproduces the major features of the observed mesoscale variability in the Gulf of Lions and the large eddies evolution in the Algerian Basin.

The seasonal evolution of circulation in the Gulf of Lions and processes of spreading of newly formed intermediate deep waters in the post-convection period is studied for years 1987 and 1992. The model results are compared with data from observations. It is shown that the instability of the transition zone between old and newly formed deep waters, which takes place after the violent mixing stages of the deep convection, leads to collapse of the mixed patch and formation of mesoscale eddies. Some of these eddies propagate out of the Gulf of Lions transporting deep waters into the Algerian Basin. The rest of the mesoscale eddies filled with newly formed deep waters remain in the Gulf of Lions, and tend to merge and enlarge. After the cyclonic eddies reach the Algerian Basin they interact with the intense mesoscale field existing there.

The energy analysis shows that the winter and spring are seasons of intensified baroclinic instability of the mean flow in the two regions of interest - the Gulf of Lions and Algerian Basin. The kinetic energy is released by baroclinic instability in spring and summer. The spring spectra in the two

regions have maximums at horizontal scales of about 80-100 km which is the typical scale of the eddies in the model. These eddies propagate a cyclonic circuit. The resulting eddy-induced mass transport is directed in the Gulf of Lions towards the Gibraltar Strait. Equivalently we can argue the intermediate and deep waters conveyor belt of the Western Mediterranean Sea is eddy driven.

## 1. Introduction

The processes of the water mass formation and transport in the Western Mediterranean were intensively studied during the recent two decades. A comprehensive review of this work is given in Millot (1987, 1994, 1999), where the circulation features of the Western Mediterranean and their role on the water mass transport are discussed mainly from an observational point of view. In particular it was demonstrated

that the mesoscale variability has an important impact on the water mass transport in the Western Mediterranean. At the same time the available data are rather sparse in time and space and some important questions about the water mass transport in the Western Mediterranean remain still open. In particular, it is well known that the Mediterranean outflow to the North Atlantic involves waters which are formed by the deep convection in the Gulf of Lions (Kinder and Parilla, 1987). However their pathway from the north-west Western Mediterranean to the Strait of Gibraltar is still not well studied (see Schott *et al.* 1996 for more discussions).

In this paper we study the impact of the eddy variability on the processes of formation and propagation of the Western Mediterranean water masses by using an ocean general circulation model. Four Western Mediterranean water masses will be of particular interest in our study - the Modified Atlantic Water (MAW), the Modified Levantine Intermediate Water (MLIW), the Winter Intermediate Water (WIW), and the Western Mediterranean Deep Water (WMDW). The surface characteristics in the basin are strongly influenced by the MAW, which originates from the Atlantic waters inflow through the Gibraltar Strait and propagates eastward along the African coast (see Fig. 1). The MAW occu-

pies usually the upper 100 m layer and is characterized by salinity in the range from 36.5 psu at Gibraltar and 38 - 38.3 psu in the northern Western Mediterranean, and by temperatures below the mixed layer of about $14^o - 15^o$C (Millot, 1999). The Levantine Intermediate Water (LIW) forms in the eastern most part of the Mediterranean Sea and enters the Western Mediterranean through the Sicily Strait (see Fig. 1), where it has salinity of about 38.7 psu and temperature maxima higher than $14^o$C. In the Western Mediterranean this water mass, which will be referred hereafter as the Modified Levantine Intermediate Water (MLIW), propagates at intermediate layers, between 300 and 500 meters and is transformed by processes of vertical and horizontal mixing. The MLIW follows a counter clockwise circuit in the Tyrrhenian Sea and through the Sardinia channel enters the Algerian Basin.

The WIW and the WMDW form during the winter convection in the northern Western Mediterranean. The WIW, which has an important impact on the variability of the Western Mediterranean (Millot, 1999), is defined by Salat and Font (1987) as the water mass with temperature between $12.5^o$C and $13^o$C and salinity 38.1-38.3. The WIW is thought to be formed on the continental shelf and propagate in the whole basin below the MAW (see Pinot*et al.*, 1995). The WMDW formation in the Gulf of Lions (see Fig. 2) was observed by the MEDOC experiment (MEDOC group, 1970) in early 1969. Since that time several more observational studies reported deep waters formation in the region $3^o30'E \leq \lambda \leq 6^oE$; $41^oN \leq \varphi \leq 43^ON$, which now is commonly referenced as the MEDOC area (see Gascard, 1978). The deep convection usually reaches great depths over the local topographic feature of the Rhone fan (see Fig. 2) due to strong winter heat losses and specific local oceanographic factors which destabilize the water column.

The spreading of the water masses in the Western Mediterranean, including those which form in the Western Mediterranean (the WIW, and the WMDW) and those which enter the Western Mediterranean through the straits of Sicily (the MLIW) and Gibraltar (the MAW) depends in a complex way upon the variability of the circulation in the basin. The physical processes, which determine the transport and transformation of the water masses in the Western Mediterranean are related to three different and interactive scales of the circulation in the Mediterranean Sea (see Robinson and Golnaraghi, 1994), which are the basin scale, sub-basin scale and mesoscale. The basin scale circulation of the Mediterranean Sea, which is shown on Fig. 1, is composed of one zonal thermohaline cell in the whole basin and two meridional thermohaline cells in the Western and Eastern Mediterranean respectively. The zonal cell is formed by the surface eastward flow of MAW and a westward transport of LIW in the Eastern Mediterranean and the MLIW in the Western Mediterranean at intermediate layers. The two meridional cells are driven directly by the processes of deep convection in the Gulf of Lions in the Western Mediterranean and in the Adriatic Sea in the Eastern Mediterranean respectively. Recently the Eastern Mediterranean meridional cell received a contribution from the Aegean Sea deep waters, also called the Eastern Mediterranean Transient (Roether *et al.*, 1996).

The sub-basin scale circulation of the Mediterranean Sea is composed of boundary currents, open ocean jets and gyres. A major sub-basin scale boundary current in the Western Mediterranean is the eastward Algerian Current along the African Coast. This current reveals a relatively intense mesoscale variability (see Ayoub *et al.*, 1998), which may have an important impact on the MAW and MLIW spreading in the Western Mediterranean ( Fuda *et al.*, 2000; Millot and Taupier-Letage, 2005). The major sub-basin scale gyre of the

Western Mediterranean is the Gulf of Lions cyclonic gyre in the northern part of the basin. The latter is composed in its northern part of the Ligurian- Provencal current along the coastal shelf break of the Ligurian-Provencal basin and the Catalan Sea (Millot, 1999). In the south, the Gulf of Lions gyre is delimited by the Balearic current which hugs the northern side of the Balearic Islands (Pinot *et al.*, 2002). Eastward of the Balearic islands the current limiting the gyre gyre has not been well defined in the literature except for the West Corsica Current (Millot, 1999) that closes the gyre in its eastern side. It is worth mentioning that also the western border of the gyre is not well defined probably because the mesoscale variability is very intense and makes it difficult to recognize a true southern border. The previous model and data studies showed that the mesoscale variability in the Ligurian-Provencal basin strongly influences the processes of the WMDW formation and spreading, thus revealing a strong interaction between the basin scale and sub-basin scale circulation (see Swallow and Caston, 1973; Gascard, 1978; Madec *et al.*, 1996).

In this article we study the processes of deep and intermediate waters formation and spreading in the Western Mediterranean, the impact of the eddy variability on the deep and intermediate water mass pathways and on the basin scale zonal and meridional circulation shown in Fig. 1. Detailed review of previous studies of these problems may be found in Marshall and Schott (1999) and Millot (1999). Throughout the text we will use these articles in the verification and interpretation of our results.

We use an ocean general circulation model, which is set up for the whole Mediterranean Sea and is forced by interannually variable surface momentum and heat fluxes (see section 2). In section 3 we compare the model results with available data about the deep convection in the Gulf of Lions. Section 4 describes the post-convective variability in the

MEDOC area. In section 5 we discuss the mesoscale variability in the Algerian Basin as simulated by the model. Section 6 presents the analysis of eddy generation processes and and energetics. In section 7 we discuss the impact of the mesoscale variability on the water masses formation and transport.

## 2. The model

The model used is the Modular Ocean Model, with horizontal resolution of $\frac{1}{8}^o \times \frac{1}{8}^o$ and 31 vertical levels. The model set up, which is described in details in Demirov and Pinardi (2002), is based on the previous works of Roussenov *et al.* (1995) and Korress *et al.* (2000). Horizontal mixing is biharmonic with tracers diffusion coefficients equal to $1.5\text{x}10^{10} m^4/s$ and the viscosity coefficient is $5\text{x}10^9 m^4/s$. The vertical mixing is parameterized by constant vertical turbulent coefficients $0.3\text{x}10^{-4} m^2/s$ for tracers and $1.5\text{x}10^{-4} m^2/s$ for momentum. A standard convective adjustment is used to remove the static instability in the water column.

The surface forcing is computed in an interactive way with 6 hourly ECMWF (European Center for Medium Range Weather Forecast) atmospheric reanalysis and analysis fields and Sea Surface Temperature (SST) from the model (see Castellari *et al.*, 1998, 2000). The ECMWF reanalysis is used for the period 1979-1993 and ECMWF analysis for 1994 - 2000. The model is first run for 7 years with perpetual monthly mean forcing to reproduce the seasonal cycle in the basin.

The model results are from two different model runs - the first one for the period from 1979 to 1993, and the second one from 1993 to 1999. The two runs are initialized by the solution of the perpetual run. Demirov and Pinardi (2002) presented model simulations for the period of time from 1979 to 1993. The analysis of model results indicated in

particular, presence of a large drift in the solution for the intermediate and deep layers. In order to diminish the effect of the model drift on the results for the years 1993 to 1999, the second simulation is initialized on January 1, 1993 by the solution of the perpetual run.

## 3. Deep convection in the Gulf of Lions: model simulation of the 1987 and 1992 events

In this section we analyze the model results for two particular years - 1987 and 1992. Extensive descriptions of the deep water formation in the Gulf of Lions for these years are available from the previous studies of Schott and Leaman (1991), Leaman and Schott (1991), and Schott *et al.* (1996).

The data and our model simulations suggest that in 1987 the violent mixing phase occurred in the Gulf of Lions already in late January. Thus we show the preconditioning at the beginning of January 1987 simulated density field (Fig. 3) does not indicate yet the presence of deep convection. In Fig. 4 are shown velocity and density fields for the same depths and period, i.e. 1-3 January, but for year 1992. The circulation in the surface and intermediate layers over the shelf slope of the Gulf of Lions, is dominated by the LPC during the two years, 1987 and 1992 (see Figs. 3a,b, and 4a,b). A local intensification of the cyclonic flow is observed in the area over the Rhone fan, where a cyclonic vortex (C1) forms during the preconditioning phase. It is stronger in 1992 (Fig. 4a) and relatively weak in 1987 (Fig. 3a). For the two years the vortex C1 is hardly seen below 1000m (see Figs. 3c,d, 4c,d).

Previous studies noticed that the presence of C1 mesoscale vortex in the surface layer, which is exposed to the surface cooling, has an important impact for the deep convection.

Swallow and Caston (1973) observed this intense cyclonic vortex during the preconditioning phase of the deep convection in MEDOC area. Madec *et al.* (1996) reproduced the vortex in their numerical simulations of the Gulf of Lions, and showed that it has an important impact on the deep convection. Legg and McWilliams (2001) demonstrated, that even in the case of horizontally homogeneous surface forcing the deep convection area tends to localize in areas with relatively small horizontal extensions in the central part of the mesoscale vortices.

In the case of the MEDOC area the presence of the cyclonic vortex C1 is an essential component of the preconditioning, which determines the location of deep convection. It modifies the density field, producing a relatively strong uplifting of the isopycnal surfaces in the upper 1000 m (see Figs. 3a,b,c and 4a,b,c). The preconditioning of the water column and the strong Mistral winds in the area of vortex C1, which is very close to the Rhone valley, makes the conditions there favorable for the violent mixing phase of the deep convection.

Beyond the vortex over the Rhone fan, two other mesoscale eddies (C2 and C3), which form by the instability of the cyclonic Ligurian Provencal Current are observed in 1987 and 1992 north-eastern and and south-eastern of the Rhone fan (see Figs. 3c,d and 4c,d). Contrary to the vortex C1, these eddies are well developed also at intermediate and deep layers (see Figs. 3b,c,d, and 4 b,c,d). We will refer to these cyclonic eddies hereafter as the deep cyclonic eddies of the MEDOC area.

Even though they have variable size and positions, the three eddies (C1, C2, C3) tend to persist during the two years. They are positioned inside the Gulf of Lions cyclonic gyre and show some relation to the topographic features. C1 forms always over the Rhone fan.

The deep cyclonic eddies C2 and C3 develop in the two deep areas within the cyclonic gyre and separated by the Rhone fan. The physical processes of formation of these eddies are discussed in more details in sections 4 and 6.

The observational studies of Schott and Leaman (1991) and Schott *et al.* (1996) indicated that the deep convection in 1987 and 1992 had a different intensity and horizontal extension. The shaded area on the upper panel of Fig. 5 shows the horizontal extension of the mixed patch in 1987, where the water column was homogenized down to depths of 2000m (see Fig. 5, lower panel). In the 1992 the convection was observed in a small area (see Fig. 6, upper panel) and down to 1500 - 1800 m depth only (see Fig. 5, lower panel). A vertical meridional section of the model density distribution along the $5^oN$ is shown on Fig. 7 for the "violent mixing" phase of the deep convection events in 1987 and 1992. The position of the deep convection in the two cases is concomitant with the position of cyclonic vortex C1 over the Rhone Fan on Figs. 3a, 4a. The density distribution suggests that the water column in the MEDOC area is homogenized in 1987 down to 2000m depth (see Fig. 7a). In 1992 (see Fig. 7b) the vertical mixing reaches maximum depths only of about 900m. The position and depth of deep convection in 1987 in the model results correspond well to the observations of Leaman and Schott (1991) for 1987 (Fig. 5). The model underestimates the depth of the deep convection in 1992 (see Fig. 6) and the density of newly formed deep waters in the two years. Castellari et al, 2000 showed that the intensity of the deep convection and the properties of newly formed deep water are strongly sensitive to the uncertainties in the surface forcing. The ECMWF reanalysis which we use as forcing for our model study has a horizontal resolution of about 100km. The error in the characteristics of newly formed deep water is a result of uncertainties in

the surface forcing. At the same time this error (of about 0.05 $kg.m^{-3}$) is relatively small with regard to the horizontal contrast of density created by the deep convection and we assume that it is not significant for the post-convective evolution of the circulation in the MEDOC area which is discussed in the following sections.

## 4. Post-convective variability of the MEDOC area

The two deep convection events in 1987 and 1992 had different intensity. Correspondingly our results suggest that the post-convective evolutions of the newly formed deep waters in these two years were also different. Here we use the model results from the 1987 run to study the post-convective evolution of newly formed WMDW. The results from the 1992 simulations are used to identify the changes in the regime of circulation in the Gulf of Lions during the years of weak winter convection (1992) with respect to the circulation in years of intense WMDW formation (1987).

The homogenization of water column during the violent mixing stage, which diminishes the Rossby radius of deformation, favors baroclinic instability of the flow (see Legg and McWilliams, 2001). The flow during the first days and weeks after the deep convection is dominated by relatively small eddies (not shown here) which tend to merge and enlarge.

In 1987 some small eddies with size of few tens of km are observed in the velocity and density fields during March(see Fig. 8a) but the flow is generally dominated by the large scale cyclonic LPC. An eastward branch of LPC forms during this year at latitude of about $40^o$N. This branch gives origin to the rim current of the Gulf of Lions in its southern extension region. . The latter is commonly referenced also as transition zone (Testor and Gascard, 2003). The surface density and velocity fields evolution during the following months (Figs. 8b-8f and 9b-9f) reveal two major tendencies: a) the weakening

of the horizontal density anomalies in the MEDOC area due to the surface heating; and b) intensified intrusions of MAW from the Algerian Basin along the Western Corsica coasts. These tendencies lead to the intensification of the circulation along Balearic islands and of the Western Corsica Current.

The rim current is the dominant circulation feature in the intermediate layer during March - May of 1987 (Figs. 10a,b). Though the instability of the cyclonic rim current and mesoscale eddies produce lateral outflow, the area of the newly formed dense intermediate waters remains compact until June, 1987. Thus the mixed patch at intermediate layers tends to persist in the model solution until early summer. In 1987 the mixed patch breakdown in July and splits in several smaller eddies. In the following months, the eddies in the south-eastern part of the mixed patch interact and merge with surrounding eddies . As a result a new eddy (C4) forms at the southern edge of the MEDOC area, which in October (Figs. 10e,f), tends to propagate southward in to the Algerian Basin (see also section 6). The eddies which form after the collapse of the mixed patch in its northwestern part tend to merge and enlarge, and organize into a new area with cyclonic but weaker circulation. In 1992 (Fig. 11), when the winter convection is relatively weak and newly formed intermediate waters are of relatively small amount, the features of density and velocity described above are not well represented. During this year the area of newly formed intermediate waters split in two smaller areas already in April and then slowly dissipate due to the lateral exchange.

The circulation in the deep layers in March of 1987 (Fig. 12a) shows the south-eastern part of the rim current located in the transition zone of the intermediate layers. This cur-

rent is less stable than in the intermediate layers and already in April, May (Figs. 12b,c) C4 appears north of Majorca, containing the newly formed WMDW.

## 5. Simulated eddy variability in the Algerian Basin

The Algerian Basin (see Fig. 2) is the region where the WMDW outflow can occur after the convection processes. This implies a meridional circulation of the WMDW, as depicted on Fig. 1. According to Fuda *et al.* (2000) "the Algerian Current generally appears as a series of eddies, mainly anticyclonic a few 10 of km in diameter, propagating downstream at 3- 5 km/day". Millot *et al.* (1997) defines two kinds of mesoscale eddies of the Algerian Current. Most of the Algerian eddies are relatively small, with few tens of kilometers horizontal extension, and shallow, only in the surface 200 m layer. Following Fuda *et al.* (2000) we will refer them as *serial* or *surface eddies*. They have a strong signal only in the velocity field of the surface MAW layer. The second kind of Algerian eddies called *events* (Fuda *et al.*, 2000) are deep and induce strong currents at all depths. Near the African coast, the events tend to propagate eastward, and approaching the Sardinian channel they turn northward (Millot, 1985; Vignudelli, 1997). Then they move back westward in to the deep part of the basin (Benzohra and Millot, 1995; Millot *et al.*, 1997). The propagation of these events along this cyclonic circuit may last as long as 3 years (Puillat *et al.*, 2002).

Here we discuss the simulated eddy variability in the Algerian Basin for the period of 1997 and 1998. This particular period was chosen because it covers the time period of the ELISA-4 experiment in the Algerian Basin (see Millot and Taupier-Letage, 2005). During this time period two of the eddies are relatively persistent and following Millot

and Taupier-Letage (2005) they will be refereed here as eddy 96.1 and eddy 97.1 (see Fig. 13).

In the model solution, the eddies of the Algerian Current are predominantly anticyclonic. Fig. 14 shows the temperature and velocity fields in the surface layer averaged over four 3 days periods of time. During the first period 27-30 July, 1997 (see Fig. 14a) the model solution shows a large anticyclonic eddy which is called 97.1 in the data (Fig. 13). The eddy called 96.1 in March 1998 in the observations is probably instead the remnant of 96.2 which has shifted northward and interacted with southern rim of the Gulf of Lions Gyre. According to the observations (see Figs. 13d,f,h) the anticyclonic eddies 96.1 and 97.1 propagate during the period March-June, 1998 with velocities, which are higher than their estimations by the model (see Figs. 14b,c,d and Figs 15b,c,d). We argue that the eddy indicated with 96.1 in May 1998 could be simply another eddy, as our simulation shows. Observations tend to underestimate the presence of 96.2 which is always present in our simulation. Given the errors in the observational resolution and the model simulation we conclude that the model reproduces reasonably well the intensity, position and presence of eddies in the Algerian Basin during this period.

Comparing the surface fields (Figs. 14) with that at intermediate layers (Figs. 15) one can remark that the anticyclonic eddies in the western part of the Algerian Basin are surface intensified and are relatively weak at intermediate layers. Moving eastward these eddies intensify also at intermediate layers. The strongest eddy induced currents at intermediate layers are observed when the anticyclonic eddies approach the western coast of Sardinia. This intensification of intermediate circulation is concomitant with the process of trapping by the eddies of MLIW, which enters the Algerian Basin through

the Sardinia Channel. Going northward along the Sardinia coast the anticyclonic eddies remain strong at intermediate layers and weaken at the surface. This is very well seen in eddy 96.2 which in 1998 gradually weakens at the surface and intensifies at intermediate layers from March to June.

## 6. Eddies of the Algerian and Provencal Basins: generation, scales, and energetics

In the previous sections we have discussed two different aspects of the eddy variability in the Western Mediterranean. The first one is related to the processes of deep water formation in the MEDOC area and spreading of the WIW and WMDW, and the second one is related to the mesoscale variability in the Algerian Basin. These two problems, which are commonly studied separately, reveal many similarities and interconnections. In particular, the variability of the two areas - the northern Western Mediterranean and the Algerian Basin are strongly influenced by the mesoscale eddies. This result is also supported by existing observational studies discussed above. In this section we discuss the physical processes that govern the generation and evolution of Western Mediterranean eddies.

The sinking and spreading, which occurs after the violent mixing, is the less studied stage of the deep convection in the MEDOC area. During this stage the newly formed deep waters propagate outside the MEDOC area. Previous model (Jones and Marshall, 1993; Madec *et al.*, 1991, 1996) and observational (Gascard, 1978) studies suggest that the mesoscale eddies generated by the instability of the rim current play an important role for the mixing between the area of deep convection and the stratified waters outside the region of deep convection. The model results discussed in section 4 suggest also that

the processes of geostrophic adjustment, baroclinic instability and mixed patch breakdown have a strong impact on the mixed patch water masses spreading. In particular our model results show that the mixed patch is relatively stable during the spring and only in early summer it breakdowns into several eddies. Similar conclusion about the post-convective behavior of the mixed patch is made in the previous studies of Legg and Marshall (1993, 1998). These authors demonstrated that the mixed patch formed after the deep convection tends to break down into mesoscale "clumps", which transport efficiently the newly formed cold waters away from the deep convection areas. Legg and Marshall (1993) have shown that when the rim current is not present the mixed patch breaks down on time scale of few days. In particular, Madec *et al.* (1996) demonstrated that the barotropic cyclonic current around the MEDOC area suppresses the baroclinic instability during the time period immediately after the deep convection. Legg and Marshall (1998) showed that this impact of the ambient flow on the stability of the mixed patch depends strongly on the intensity of the rim current. If the cyclonic flow is not strong enough, the baroclinic potential vorticity anomaly created by the deep convection continuously increases and generates baroclinic instability. If however the pre-existing barotropic potential vorticity anomaly is energetic enough, it may suppress the baroclinic instability. Legg and Marshall (1998) suggested that in this case the ambient cyclonic flow is "self-perpetuating", i.e. the cyclonic circulation inside the deep convection area reinforces the ambient flow, while the intensified rim current suppresses more efficiently the baroclinic instability. In our model simulations this "self-perpetuating stage" is observed in the post-convective development of the mixed patch before its breakdown in the beginning of summer. The model solution (see section 4) suggests that during this stage the eddies within the mixed patch tend to

merge and enlarge and the cyclonic flow around the convection area intensifies during this stage.

From the discussion of the model results presented above it follows that the post-convective circulation in the Gulf of Lions reveals a strong interaction between the mean and eddy flow. In order to quantify this interaction here we estimate the rate of conversion between mean and eddy energy in the Gulf of Lions and Algerian Basin. In our calculations we represent each model variable as a sum of its mean in time value and an eddy perturbation:

$$(u, v, w, T, S) = \left(\overline{u}, \overline{v}, \overline{w}, \overline{T}, \overline{S}\right) + (u', v', w', T', S')$$

The density field($\rho$) is divided in three parts - steady (motionless) state ($\tilde{\rho}$), mean ($\overline{\rho}$) and perturbation ($\rho'$):

$$\rho(x, y, z, t) = \tilde{\rho}(z) + \overline{\rho}(x, y, z) + \rho'(x, y, z, t)$$

and $s(z) = \frac{\partial \tilde{\rho}}{\partial z}$ is the basin mean vertical gradient of $\tilde{\rho}(z)$. The mean available potential energy $APE_m$, eddy available potential energy $APE_e$, mean kinetic energy $KE_m$ and eddy kinetic energy $KE_e$ are defined as follows (see Lorenz, 1955):

$$APE_m = \frac{1}{V}\int\int\int -\frac{1}{2} g\rho_0 \frac{\overline{\rho}^2}{\frac{\partial \tilde{\rho}}{\partial z}} \quad , \quad APE_e = \frac{1}{V}\int\int\int -\frac{1}{2} g\rho_0 \frac{\overline{\rho'^2}}{\frac{\partial \tilde{\rho}}{\partial z}}.$$

$$KE_m = \frac{1}{V}\int\int\int \frac{1}{2}\rho_0 \left(\overline{u}^2 + \overline{v}^2\right) \quad , \quad KE_e = \frac{1}{V}\int\int\int \frac{1}{2}\rho_0 \left(\overline{u'^2} + \overline{v'^2}\right).$$

The evolution of $KE_m, KE_e, APE_m$ and $APE_e$ depend (see Pinardi and Robinson, 1986) on the surface energy fluxes, vertical and horizontal energy advection and diffusion, and the rates of conversion between these four components of model energetics. The conversion rate between $APE_m$ and $APE_e$ is given by:

$$T_1 = -\frac{g}{s}\left[\overline{u'\rho'}\frac{1}{a\cos\phi}\frac{\partial \overline{\rho}}{\partial \lambda} + \overline{v'\rho'}\frac{1}{a}\frac{\partial \overline{\rho}}{\partial \phi} + \overline{w'\rho'}\frac{\partial \overline{\rho}}{\partial z}\right]$$

and characterizes the intensity of the processes of baroclinic instability. When $T_1$ is negative the potential energy of mean flow is extracted by the processes of baroclinic instability into eddy potential energy. The conversion rate between $KE_m$ and $KE_e$ is:

$$T_2 = \frac{1}{a\cos\phi}\left(\overline{u'^2}\frac{\partial\overline{u}}{\partial\lambda} + \overline{u'v'}\frac{\partial\overline{v}}{\partial\lambda} + \overline{u'v'}\cos\phi\frac{\partial\overline{u}}{\partial\phi} + \overline{v'^2}\frac{\partial\overline{v}\cos\phi}{\partial\phi}\right) + \overline{v'w'}\frac{\partial\overline{v}}{\partial z} + \overline{u'w'}\frac{\partial\overline{u}}{\partial z}$$

and characterizes the intensity of processes of barotropic instability. When $T_1$ is negative the kinetic energy of mean flow ($KE_m$) is converted into eddies kinetic energy ($KE_e$). In opposite when $T_1$ and $T_2$ are positive, they estimate the intensity of conversion of eddies energy into the energy of mean flow. Tables 1-6 show an estimation of the mean ($APE_m$) and eddy ($APE_e$) Available Potential Energy, mean ($KE_m$) and eddy ($KE_e$) kinetic energy and the conversion rates between mean and eddy energy for the period of time from 1981 to 1990. The elements of energy balance shown on Tables 1-6 are computed for surface ($0m < z < 250m$), intermediate ($250m < z < 500m$) and deep ($z > 500m$) layers.

The surface forcing over the Western Mediterranean is strongest in the winter season. During this season there is a strong increase in the $APE_m$ for the two basins, the Algerian Basin and the Gulf of Lions. The increase of $APE_m$ in the Gulf of Lions is partly due to the intensified surface APE flux, and partly due to intensified conversion of $KE_m$ to $APE_m$. In the Algerian Basin the major factor for the winter $APE_m$ increase is the intense lateral $APE_m$ advective flux through the Gibraltar Strait during this season. The transformation of $APE_m$ to $APE_e$ through the processes of baroclinic instability in the surface layer for the two regions is strongest also in winter (Table 1). In the intermediate and deep layers the seasonal variability of $APE_m$ is much smaller than in the surface layer. The baroclinic instability in these layers is strongest in the spring. The conversion

of the kinetic energy of mean flow to eddy kinetic energy in all of the layers has a smaller impact on the generation of eddy energy than the processes of baroclinic instability. In some of the cases (like summer season in the Algerian Basin), the conversion term $T_2$ is directed from eddy to mean flow.

From the results presented in Table 1 we may conclude that the dominant mechanism for the formation of mesoscale eddies in the Western Mediterranean are the processes of baroclinic instability, which convert $APE_m \rightarrow APE_e \rightarrow KE_e$ and are strongest in winter and spring. The baroclinic instability in the surface layer of the Algerian Basin (Table 1)is much stronger than that for the Gulf of Lions (Table 4). On the other side the eddy energy production by baroclinic instability in the intermediate and deep layers is much stronger in the Gulf of Lions (Tables 2,3) than in the Algerian Basin (Tables 5,6). We have shown that eddies in the Algerian and Gulf of Lions basins are formed by baroclinic instability. We proceed now to a scale analysis of the size of the eddies produced as a function of the season and thus the different WMDW formation phases.

The three days averaged spectrum of barotropic kinetic energy in the Gulf of Lions are shown on Fig. 16 for four periods of 1987: winter (JFM), spring (AMJ), summer (JAS) and autumn (OND). These periods coincide with the major stages in the evolution of the MEDOC area described in sections 3 an 4, i.e. (1) violent mixing in winter, (2) "self-perpetuating" stage of the post-convective evolution of the mixed patch in spring, (3) mixed patch breaks down in summer, and (4) spreading of newly formed deep waters in autumn. The kinetic energy spectrum is normalized to satisfy $\int_0^\infty E(k)dk = \overline{\frac{(u_b^2+v_b^2)}{2}}$, where $\overline{\frac{(u_b^2+v_b^2)}{2}}$ is the area mean kinetic of energy of vertically mean flow.

Winter energy spectrum in the Gulf of Lions in Fig. 16a is characterized by high values of spectral densities in the whole spectral interval. The variance is relatively strong in high wave number interval $2\pi/k < 50km$. According to the linear instability theory for continuously stratified fluid, the fastest growing mode is at wavelength of $\gamma = 3.9Ro$, where Ro is the internal radius of deformation (see Cushman-Roisin, 1994). Ro during this season changes from 5 km during the period of winter convection to about 15 km at the beginning of the spring (see Robinson and Golnaraghi, 1994). Correspondingly the wave numbers of fastest growing modes evolve within the interval from 15km to 60km and the spectrum is highly variable within this interval. This spectral interval will be refereed hereafter as to the *interval of baroclinic instability*. The variance within the interval of baroclinic instability is relatively high during the all seasons but larger during the winter. During the period April-June (Fig. 16b) a spectral maximum develops at $2\pi/k_0 \approx 70km$. As discussed above during this season, the eddies generated within the mixed patch by the processes of baroclinic instability tend to merge, enlarge and intensify. Correspondingly the dominant scale in the energy spectrum also increases towards $2\pi/k_0$. The mixed patch in July collapses into smaller scale eddies. The spectral maximum at $k_0$ decreases during the the summer and at the end of the season it almost disappear (Fig. 16d). Correspondingly the spectral density increases at $2\pi/k_1 \approx 50km$ which is within the interval of baroclinic instability.

The barotropic kinetic energy spectrum for the Algerian Basin (Fig. 17) reveals a a different structure from the Gulf of Lions because the Ro is now always between 10 and 15 km. Thus 15 km eddies are not likely to occur by baroclinic instability and the spectral

density values decrease rapidly below 60 km spatial scales (Fig. 17). However, in this basin a new process seems to emerge from the spectral analysis.

In all of the seasons the spectrum above 60km scales is close to -5/3. This slope is predicted by the 2-D turbulence spectrum slope for the interval of inverse cascade.

The theory of 2-D quasi-geostrophic turbulence predicts that in a flat bottom f-plane ocean the energy-containing scales increase due to the inverse cascade until they reach the domain size. If however, there exists a mechanism restricting the size of the eddies, a kinetic energy peak develops at the scales at which this mechanism is more effective. (Larichev and Held, 1995). The mechanisms that may halt the inverse cascade are related to $\beta$-effect, scattering by topography, or boundary layer friction. On $\beta$-plane, the inverse cascade is halted at the Rhines scale $k_R = (\beta/V)^{\frac{1}{2}}$ for which the velocity scale of eddies propagation V becomes equal to the Rossby waves phase speed (see Rhines, 1975). The definition of Rhines scale includes implicitly the assumption that at large scales there exist an efficient mechanism for dissipation of the energy cascaded towards $k_R$. Otherwise the energy in dissipation-free ocean flow would keep accumulating at $k_R$. The Rhines scale for the Western Mediterranean is $2\pi/k_R \approx 500km$ and is larger than maximum horizontal extension of deep part of the basin, which is about 400 km (see Fig 2). Additionally the size of the eddies in the Gulf of Lions and Algerian Basin are limited by the processes of dissipation which depend in a complex way by the scattering by topography, lateral and bottom friction. The energy spectrum suggest that these processes halt the inverse cascade at about $2\pi/k \approx 70km$ in the Gulf of Lions and at about $2\pi/k \approx 110km$ in the Algerian Basin.

## 7. Mean and eddy induced water mass transport in the Western Mediterranean

The zonal cell of the thermohaline circulation in the Western Mediterranean consists of a surface westward transport of MAW and westward transport of MLIW. While the Algerian Current and the paths of the surface MAW are well studied, the results from studies of the MLIW and WMDW transport in the Western Mediterranean are less known.

Our model results for year 1987 show that the eddies with scale of about 100 km dominate the flow in the deep and intermediate layers of the Western Mediterranean. One can anticipate under the conditions of relatively weak mean flow, the eddy-induced transport may potentially play an important role for the water mass spreading. At the same time the simulations of 1992 suggest that during years with weak convection the eddy activity in the MEDOC are is also weak. Here we try to answer the question how strong is the eddy induced transport with respect to the mean mass transport.

The eddies influence the time-mean transport in two ways. One way is rectification of the mean flow. This effect of the eddies on the mean flow may be estimated if two simulations of fine- and coarse- resolution version of the same model and with the same forcing. Such a twin experiment has not been done with the present model and the rectification of the mean flow is not discussed here. We study only the second effect of eddies on the time-mean transport, which results from the correlation between density and velocity. The integral advective transport of $\sigma_t$ for the layer $z_1 < z < z_2$ is given by:

$$\mathbf{U} = \int_{z(z_1)}^{z} \mathbf{u}\sigma_t dz \quad .$$

We consider this transport to be composed of mean $\overline{\mathbf{U}}$ and eddy-induced $\mathbf{U}'$ components, where

$$\overline{\mathbf{U}} = \int_{z(z_1)}^{z} \overline{\mathbf{u}} \quad \overline{\sigma}_t dz \quad ,$$

and

$$\mathbf{U}' = \int_{z(z_1)}^{z} \overline{\mathbf{u}'\sigma_t'} dz \quad .$$

Here $\overline{\mathbf{u}}$ and $\overline{\sigma}_t$ are the time mean fields of the velocity vector $\mathbf{u}$ and density $\sigma_t$ and the $\overline{\mathbf{u}'\sigma_t'}$ is the velocity density correlation. Here we compute the mean $\overline{\mathbf{U}}$ and eddy induced $\mathbf{U}'$ transports for two layers: the intermediate layer between $250m < z < 500$, and the deep layer for $z > 500$. The stream functions for the mean and eddy induced mass transport in the two layers are then computed by inversion of the Laplasian operator $\nabla \times \mathbf{U}$, i.e.

$$\overline{\psi} = \nabla^{-2}\mathbf{k}.\left(\nabla \times \overline{\mathbf{U}}\right),$$

and

$$\psi' = \nabla^{-2}\mathbf{k}.\left(\nabla \times \mathbf{U}'\right),$$

where $\mathbf{k}$ is an unit vector directed in the vertical z-direction. . At open boundaries, the stream function is defined as a line integral of the normal to the boundary component of $\overline{\mathbf{U}}$ and $\mathbf{U}'$ correspondingly. The mean and eddy-induced transports in the intermediate and deep layers for the period time from 1981 to 1990 are shown Fig. 18.

The mean transport (Fig. 18a) in the intermediate layer of the Gulf of Lions is dominated by the cyclonic gyre, which is observed in the surface and intermediate layers of this region. An anticyclonic transport is present in the southeastern Gulf of Lions and the Algerian Basin. These two elements of the transport does not imply an outflow of intermediate waters out of the Gulf of Lions. The mean transport in the deep layer (Fig. 18b)

includes several areas of cyclonic and anticyclonic circulation. Some of these areas correspond well to the mesoscale variability discussed above. The two deep cyclonic eddies in the Gulf of Lions C2 and C3, which in 1987 and 1992 are present in the model solution with different intensity have a strong signal also in the mean transport. The same is true for the cyclonic circulation in the southeastern part of the Gulf of Lions. The circulation here is cyclonic mostly during the spring and summer when the eddy C4 tends to form. This cyclonic deep transport tends now to exchange waters between the northern and southern regions of the Western Mediterranean and we believe it is mainly due to the integrated effect of the C4 eddy movement.. The position of C4 in particular is in the southeastern Gulf of Lions in winter and moves southward in the spring.

The eddy-induced transport (Fig. 18cd) in the major part of intermediate and deep layers of the Western Mediterranean is cyclonic during the whole year. It transports MLIW cyclonically, from the Sardinia Channel along the western coast of Sardinia, Corsica and then into the Gulf of Lions. The WMDW, WIW and MLIW are transported by the eddy-induced transport out of the Gulf of Lions along the eastern coast of the Majorca Island and then westward towards the Gibraltar Strait. An anticyclonic eddy induced transport in the southern part of Algerian Basin is present in a narrow area along the African Coast.

The eddy-induced transport which probably produces transport of the MLIW and WMDW in the model solution dominate over the mean mass transport and are consistent with existing observational data, which are reviewed in Millot and Taupier-Letage (2005), and Testor et al. (2005). In particular, the latter work of Testor at al.(2005) presents results from floats trajectories observations in the Algerian Basin. The trajecto-

ries, which are shown on Fig. 19 cover the southern region of the Western Mediterranean. The data confirm presence of a cyclonic circulation in the Algerian Basin which has many similarities with the model eddy-induced transport on (Fig. 18cd). In the intermediate layer the observations show a presence of a cyclonic circulation in the area $4^oE < \lambda < 8^oE$ and $37^oN < \phi < 39^oN$ in a good agreement with the model solution (see Fig. 18c). In the deep layer the trajectories show the presence of cyclonic circulation in the area between $1^oE < \lambda < 9^oE$ and $37^oN < \phi < 39^oN$. The model suggests that a deep layer eddy induced cyclonic circulation is present also in the northern part of the Algerian Basin (Fig. 18d). The data in this area, however, are limited and the observed trajectories in this area does not allow to assess how realistic is the model result.

## 8. Discussions and conclusions

In this article we have presented a numerical model study of WMDW formation and spreading due to eddies. We tray to answer two major questions (a) what are the processes of generation of intense mesoscale variability in the Western Mediterranean; and (b) what is the relatively role of mean and eddy induced transport on the formation and spreading of intermediate and deep waters in the Western Mediterranean.

The analysis of the numerical results demonstrated that the model is capable to represent important features of the deep convection in the Gulf of Lions known from previous data and model studies. We have studied two cases of deep convection in the MEDOC area, that of 1987 and 1992, when the intensity of the vertical mixing was different. In 1987 the deep convection in the model solution reaches the bottom, while in 1992 it reaches only 800m. The comparison with the observations of deep convection during these years shows that the model tends to underestimate the density in the deep convection mixed

patch and the deep convection depth in 1992. This model error is shortcoming of the uncertainties in the surface forcing and of existing parameterizations of the vertical mixing in the Mediterranean.

The evolution of model solution during the "sinking and spreading" phase of the deep convection was studied for 1987 and 1992. The comparison of the circulation during these two cases suggests that circulation patterns differ significantly between years with and without deep water formation in the Gulf of Lions.

The model results suggest that the mixed patch formed during the deep convection is a stable feature, which persists during a period of several months after the deep convection events. In early summer the mixed patch, which is mainly present in the intermediate and deep layers, collapses and splits in cyclonic eddies. The cyclonic eddies in the south-eastern edge of the MEDOC area tend to intensify trapping partly newly formed intermediate and deep waters and propagates towards the Algerian Basin in late autumn. The rest of the cyclonic eddies remaining in the MEDOC area tend to merge and enlarge.

The energy analysis for year 1987 shows that the dominant process of mesoscale eddies in the Western Mediterranean is the baroclinic instability. It is strongest in winter and spring, when the available potential energy stored during the winter season is released in eddy potential and kinetic energy. At the same time the dominant spatial scale of the mesoscale eddies in the model solution (and available data) is about 100km and may reach in some cases 200km. This scale is larger than the wavelength of the fastest growing mode, which is expected to dominate the eddies formed by the baroclinic instability. The analysis of seasonal spectra of barotropic energy for year 1987 in the Gulf of Lions and Algerian Basin suggests that the mesoscale eddies with dominant scales of 100km are

due to the concomitant effect of baroclinic instability and 2-D quasigeostrophic inverse cascade. . In other words, the release of eddy energy by the baroclinic instability is strongest in winter and spring. In the spring and summer the eddies generated by the baroclinic instability tend to merge and enlarge towards larger scales.

The comparison of mean and eddy induced transport suggests that the eddy induced transport prevails over the mean transport in the areas which are important for the spreading of WMDW and MLIW. The mean and eddy transports are associated with the movement of eddies that trap water masses, moving within or outside the Gulf of Lions Gyre. Therefore we conclude that the eddy-driven component of the water mass transport is an important part of the conveyor belt. This component, which we call eddy driven conveyor may potentially give the answer to the question of what is the mechanism of the MLIW and WMDW transport towards to the Gibraltar. Our results suggest that both the MLIW and the WMDW follow a cyclonic path that connects the northern and southern regions of the Mediterranean, extending westward into the western Algerian basin, toward Gibraltar. This path is composed of the movement of eddies, formed by baroclinic instability, enlarged by quasigeostrophic energy cascading at large scales (merging) and trapping the selected water masses, present in the areas of their formation.

**Acknowledgments.** The work is contribution to the EU funded project MFSTEP and project 312377-05 funded by Natural Sciences and Engineering Research Council of Canada.

**References**


Ayoub, N., P.-Y. Le Traon, and P. De Mey, 1998, A description of the Mediterranean surface circulation from combined ERS-1 and TOPEX/POSEIDON altimetric data. *J. Mar. Syst.*, *18*, (1-3), 3-40.

Benzhora M., and C. Millot C., 1995. Characteristics and circulation of the surface and intermediate water masses off Algeria. *Deep-Sea Res.*, *42*,(10), 1803- 1830.

Buongiorno Nardelli, B., G. Larnicl, E.DÁcunzo, R.Santoleri, S. Marullo, and P.-Y. Le Traon, 2003. Near real time SLA and SST products durino 2-years of MFS pilot project: processing, analysis of the variability and the couplet patterns, *Ann. Geophys.*, *21*, 103-121.

Castellari, S., N. Pinardi, and K.D. Leaman, 1998. A model study of air-sea interactions in the Mediterranean Sea, *J. Mar. Syst.*, *18*: 89-114.

Castellari, S., N. Pinardi, and K. Leaman, 2000. Simulation of water mass formation processes in the Mediterranean Sea: Influence of the time frequency of the atmospheric forcing, *J. Geophys. Res.*, *105*, N 10: 24157 - 24181.

Danilov, S., and D. Gurarie, 2002. Rhines scale and spectra of the $\beta$ plane turbulence with bottom drag., *Phys. Rev. E*, *65*, 067301,1-3.

Demirov, E., and N. Pinardi, 2002. Simulation of the Mediterranean Sea circulation from 1979 to 1993: Part I. The interannual variability. *J. Mar. Syst.*, *33-34*:23-50.

Fuda, J.L., C. Millot, I. Taupier-Letage, U. Send, J.M. Bocognano, 2000.XBT monitoring of a meridian section across the western Mediterranean Sea, *Deep-Sea Res.*, *47*: 2191-2218.

Gascard, J.C., 1973. Vertical motions in the region of deep water formation. *Deep-Sea Res.*, *20*, 11: 1011-1027.

Gascard, J.C., 1978. Mediterranean deep water formation, baroclinic instability and ocean eddies. *Oceanol. Acta*, *1*, 3: 315-330.

Kinder, T.H., and G. Parilla, 1987. Yes, some of the Mediterranean Outflow does come from great depth, *J. Geophys. Res.*, *92*, 2901-2906.

Korres, G., N. Pinardi, A. Lascaratos, 2000. The ocean response to low frequency interannual atmospheric variability in the Mediterranean Sea. Part I: Sensitivity experiments and energy analysis. *J. Climate*, *13*: 705- 731.

Larichev, V., and I. Held, 1995. Eddy amplitudes and fluxes in a homogeneous model of fully developed baroclinic instability., *J. Phys. Oceanogr.*, *25*, 2285 - 2297.

Leaman, K.D, and F.A. Schott, 1991. Hydrographic structure of the convective regime in the Gulf of Lions: winter 1987, *J. Phys. Oceanogr*, *21*, N4: 575 - 598.

Legg, S., and J. McWilliams, 2001. Convective modification of a geostrophic eddy field, *J. Phys. Oceanogr*, 31, 874-891.

Legg, S., and J. Marshall, 1993. A heton method of spreading phase of open-ocean deep convection water masses, *J. Phys. Oceanogr*, 23, 1040-1056.

Legg, S., and J. Marshall, 1998. The influence of the ambient flow on the spreading of convective water masses, *J. Mar. Res.*, 56, 107-139.

Lorenz, E. N., 1955. Available potential energy and the maintenance of the general circulation. *Tellus*, *7, 2*, 157-167.

Madec G., M. Chartier, P. Delecluse, and M. Crepon, 1991. A three-dimensional numerical study of deep-water formation in the northwestern Mediterranean Sea, *J. Phys.*

*Oceanogr.*, *21*: 1349-1371.

Madec G., F. Lott, P. Delecluse, and M. Crepon, 1996. Large-scale preconditioning of deep-water formation in the northwestern Mediterranean Sea, *J. Phys. Oceanogr.*, *26*: 1393 - 1408.

Marshall, J., and F. Schott, 1999. Open-ocean convection: observations, theory, and models, *Rev. Geophys.*, *37*, 1:1-64.

MEDOC Group, 1970. Observations of formation of deep-water in the Mediterranean Sea, 1969, *Nature*, *227*:1037-1040.

Millot C., 1985. Some features of the Algerian Current, *J. Geophys. Res.*, *90*, 7169-7176.

Millot C., 1999. Circulation in the Western Mediterranean Sea. *J. Mar. Syst.*, *20*, 3-4: 423-442.

Millot C., 1994. Models and data: a synergetic approach in the western Mediterranean Sea. In P. Malanotte-Rizzoli and A. R. Robinson Eds., *Ocean Processes in Climate Dynamics: Global and Mediterranean Examples*: 143-149.

Millot C., 1987. Circulation in the Western Mediterranean. *Oceanol. Acta*, *10*, 2: 143-149.

Millot C., M. Benzhora, I. Taupier-Letage, 1997. Circulation in the Algerian Basin inferred from the MEDIPROD-5 current meters data. *Deep-Sea Res.*, *44*: 1467- 1495.

Millot C., I. Taupier-Letage, 2005. Circulation in the Algerian additional evidence of LIW entrainment across the Algerian Basin by mesoscale eddies and not by a permanent westward flow, *Prog. Oceanogr.*, (in press).

Ovchinnikov, I.M., 1966. Circulation in the surface and intermediate layers of the Mediterranean, *Oceanology*, *6*: 48-59.

N. Pinardi and A. R. Robinson, 1986. Quasigeostrophic energetics of open ocean regions, *dyn. atm. and oceans*, *10(3)*, 185-221.

Pinot, J.-M., J.L. Lopez-Jurado, and M. Riera, 2002. The CANALES experiment (1996-1998). Interannual, seasonal and mesoscale variability of the circulation in the Balearic Channels, *Progr. Oceanogr.*, *55*, 335-370.

Pinot, J.M., J. Tintore, and D. Gomis, 1995. Multivariate analysis of surface circulation in the Balearic Sea. *Prog. Oceanogr.*, *36*, 343-376.

Puillat I., I. Taupier-Letage, and C. Millot, 2002. Algerian eddies lifetime can Near 3 years, *J. Mar. Syst.*, *31*, 4, 245-259.

Rhines, P.B., 1975. Waves and turbulence on a beta-plane. *J. Fluid. Mech.*, *69*, 417-443.

Rhines, P.B., 1977. The dynamics of unsetady currents. The Sea, Vol. 6, E.A. Godberg, I.N. McCane, J.J. OBrien, and J.H. Steele, Eds., Wiley, 189-318.

Robinson, A.R., and M. Golnaraghi, 1994. The physical and dynamical oceanography of the Mediterranean Sea, In. Malanotte-Rizzoli, P., and A.R. Robinson Eds., Proceedings of NATO-ASI, *Ocean processes in Climate Dynamics: Global and Mediterranean Examples*, pp 206-306.

Testor P. and J.-C. Gascard, 2003: Large scale spreading of deep waters in the Western Mediterranean Sea by submesoscale coherent eddies, *J. Phys. Oceanogr.*, 33, 75-87.

Testor, P., U. Send, J.-C. Gascard, C. Millot, I. Taupier-Letage, K. Beranger, 2005. The Mean circulation of the southwestern Mediterranean Sea - the Algerian Gyres, *J. Geophys. Res.*, (in press)

Wolfgang Roether, Beniamino B. Manca, Birgit Klein, Davide Bregant, Dimitrios Georgopoulos, Volker Beitzel, Vedrana Kovaevi, Anna Luchetta, 1996. Recent Changes in

Eastern Mediterranean Deep Waters, *Science*, *271*, 5247, 333-335.

Roussenov, V., E. Stanev, V. Artale and N. Pinardi, 1995. A seasonal model of the Mediterranean Sea circulation. *J. Geophys. Res.*, *100*: 13515-13538.

Salat, J., and J. Font, 1987. Water mass structure near and offshore the Catalan Sea during the winter of 1982 and 1983. *Annales Geophysicae*, *5*: 49-54.

Salmon, R., 1978. Two-layer quasi-geostrophic turbulence in a simple special case. *Geophys. Astrophys. Fluid. Dyn.*, *10*, 25-52.

Schott F., and K.D. Leaman, 1991. Observations with moored acoustic Doppler current profilers in the convection regime in the Golfe du Lion, *J. Phys. Oceanogr.*, *21*: 558-574.

Schott F., M. Visbeck, U. Send, J. Fischer, L. Stramma, and Y. Desaubies, 1996. Observations of deep convection in the Gulf of Lions, northern Mediterranean, during winter 1991/92, *J. Phys. Oceanogr.*, *26*: 505-524.

Spall, M.A., 2000. Generation of strong messocale eddies by weak ocean gyres. *J. Mar. Res.*, *58*: 97-116.

Swallow,J.C. and G.F. Caston, 1972. The preconditioning phase of MEDOC 1969-I. Observations, Deep-Sea Re., Vol. 20, pp. 429-448.

Vignudelli, S., 1997. Potential use of ERS-1 and Topex/Poseidon altimeters for resolving oceanographic patterns in the Algerian Basin. *Geophys. Res. Lett.*, *24* (14): 1787-1790.

Wu P., and K. Haines, 1996. Modelling the dispersal of Levantine intermediate water and its role in Mediterranean deep water formation, *J. Geophys. Res.*, *101*, C3: 6591 - 6607.

**Figure Captions**

Figure 1. Scheme of the basin-scale circulation in the Mediterranean Sea (after Pinardi and Massetti, 2000).

Figure 2. Bottom topography in the Algerian and Ligurian - Provencal basins. The two squared areas shown in the Gulf of Lions and the Algerian Basin are the areas, where energetic analysis is performed in section 6.

Figure 3. Mean velocity and density distributions in the Gulf of Lions for the period 1-3 January, 1987 at (a)50m; (b) 500m; (c) 1000m; (d) 1800m.

Figure 4. Mean velocity and density distributions in the Gulf of Lions for the period 1-3 January, 1992 at (a)50m; (b) 500m; (c) 1000m; (d) 1800m.

Figure 5. Horizontal and vertical extent of the mixed patch in 1987 (after Schott and Leaman, 1991, and Leaman and Schott, 1991). The horizontal extent is shown on upper panel for (a) 22-29 January, (b) 23-29 January, and (c) 17-23 February, 1987. The density cross section along $5^o$E is shown on (d).

Figure 6. Horizontal and vertical extent of the deep convection area in 1992 (after Schott *et al.*, 1996). The horizontal extent and depths are plotted on the upper panel for (a) 18-22 February, 1992, (b) 23 February - 3 March, 1992, and (c) 3-9 March, 1992. The solid line indicates the horizontal boundaries of the surface convectively mixed layer. The numbers on the solid line show depth of the convection. The dashed line show the extension of the convection waters below a stratified layer and the numbers corresponding to these lines - the depth of the convection water. The density cross section along $5^o$E is shown on (d).

Figure 7.Vertical section of the density along the longitude $5^oE$ (a) 21-24 February, 1987; (b) 19-21 February, 1992.

Figure 8.Monthly mean horizontal distribution of density and velocity fields at 50 m (a) March, 1987; (b) April, 1987; (c) May 1987; (d) June 1987; (e) August 1987; (f) October, 1987.

Figure 9. Monthly mean horizontal distribution of density and velocity fields at 50 m (a) March, 1992; (b) April, 1992; (c) May 1992; (d) June 1992; (e) August 1992; (f) October, 1992.

Figure 10. Monthly mean horizontal distribution of density and velocity fields at 500 m (a) March, 1987; (b) April, 1987; (c) May 1987; (d) June 1987; (e) August 1987; (f) October, 1987.

Figure 11. Monthly mean horizontal distribution of density and velocity fields at 500 m (a) March, 1992; (b) April, 1992; (c) May 1992; (d) June 1992; (e) August 1992; (f) October, 1992.

Figure 12. Monthly mean horizontal distribution of density and velocity fields at 1500 m (a) March, 1987; (b) April, 1987; (c) May 1987; (d) June 1987; (e) August 1987; (f) October, 1987.

Figure 13. Synopsis of one-year ELISA experiment. a, c, e, g: NOAA-AVHRR infrared images. b,d,f,h scheme of the eddy field together with sampling moorings ($\Delta$), CTD (+) and XBT (x) casts. (after Millot and Taupier-Letage, 2005).

Figure 14. Horizontal distribution of temperature and velocity at 30m in the Algerian Basin in four different periods (a) 27 - 30, July, 1997 ; (b) 25-27 March, 1998; (c) 5-9 May, 1998; (d) 22 - 24 June, 1998.

Figure 15. Horizontal distribution of salinity and velocity at 360 m in the Algerian Basin (a) 27 - 30, July, 1997; (b) 25-27 March, 1998; (c) 5-9 May, 1998; (d) 22 - 24 June, 1998.

Figure 16. 3-days mean barotropic kinetic energy spectra curves of the barotropic flow in the Gulf of Lions for (a) winter, (b) spring, (c) summer and (d) autumn. The green curve shows the spectra at the beginning of each period, the red line - the spectra at the end of the period.

Figure 17. 3-days mean barotropic kinetic energy spectra curves of the barotropic flow in the Algerian Basin for (a) winter, (b) spring, (c) summer and (d) autumn. The green curve shows the spectra at the beginning of each period, the red line - the spectra at the end of the period.

Figure 18. Stream function (Sv kg/$m^3$) of the (a) mean transport in the intermediate layer; (b) mean transport in the deep layer; (c) eddy-induced transport in the intermediate layer; and (d) eddy-induced transport in the deep layer.

Figure 19. (a) Trajectories of the RAFOS floats at 600 m from July 14, 1997 until June 24, 1998. superimposed on f/H contours. (b) Trajectories of profiling floats drifting at 1200 and 2000. Arrows indicate the drift at depth during 8 days. One color of each float. (after Testor *et al.*, 2005)

file)

1987;

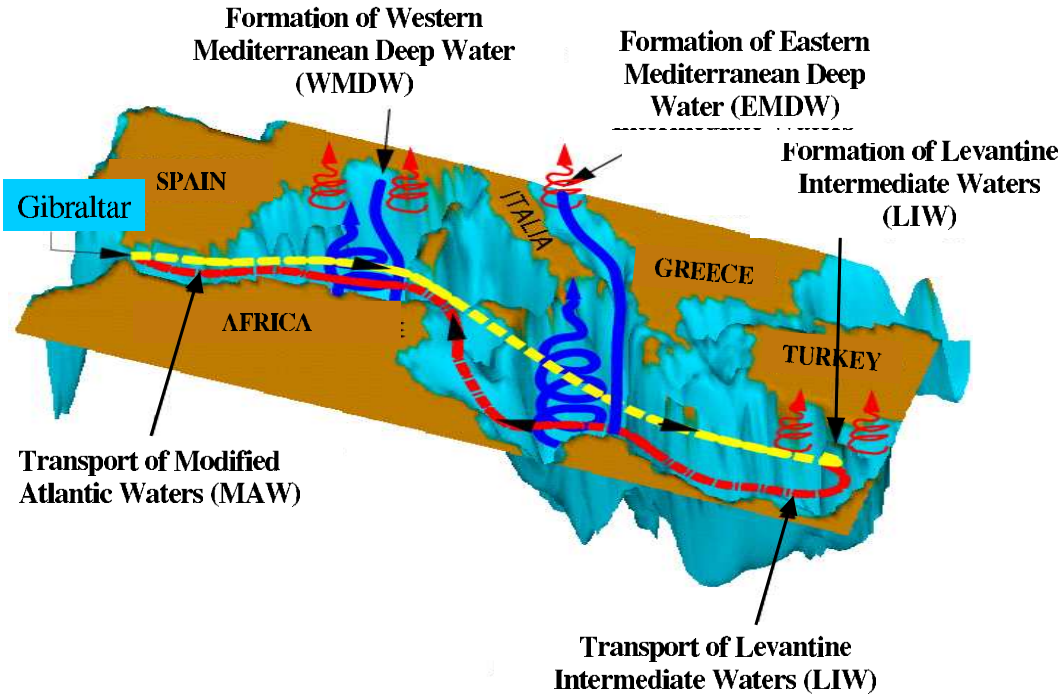


**Figure 1.** Scheme of the basin-scale circulation in the Mediterranean Sea (after Pinardi and Massetti, 2000).

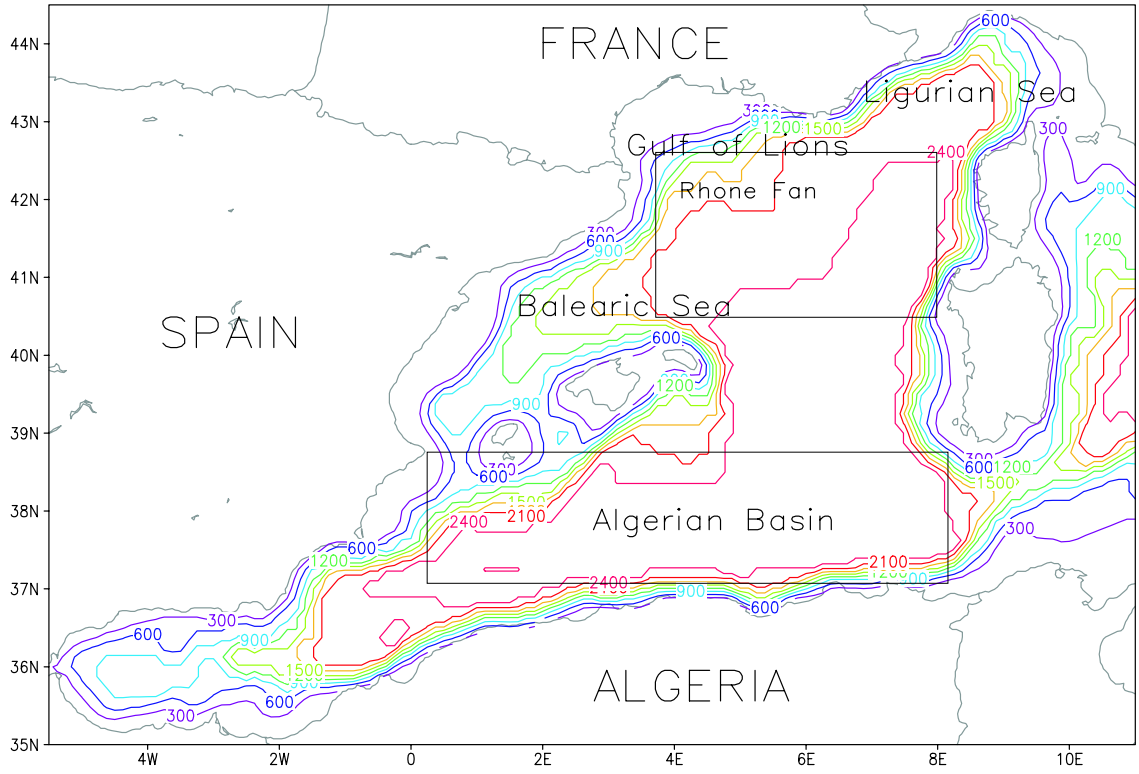


**Figure 2.** Bottom topography in the Algerian and Ligurian - Provencal basins. The two squared areas shown in the Gulf of Lions and the Algerian Basin are the areas, where energetic analysis is performed in section 6.

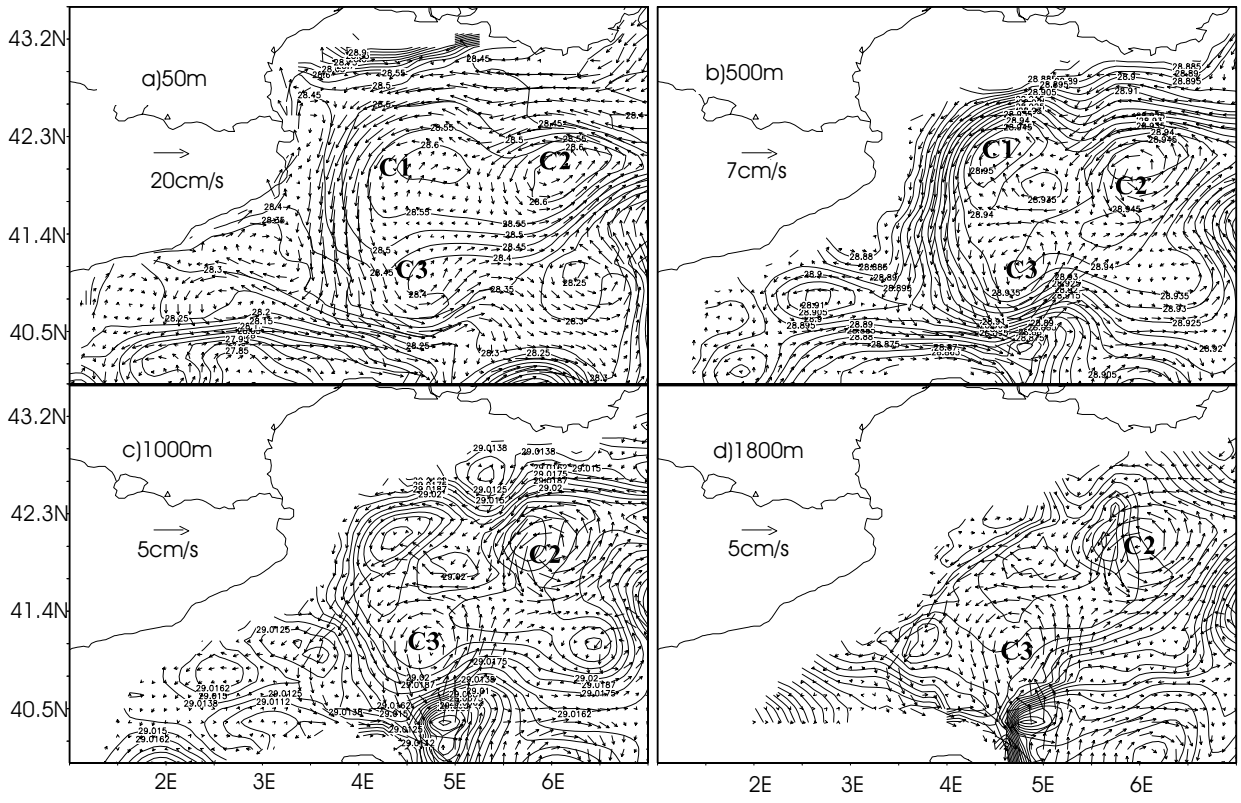


**Figure 3.** Mean velocity and density distributions in the Gulf of Lions for the period 1-3 January, 1987 at (a)50m; (b) 500m; (c) 1000m; (d) 1800m

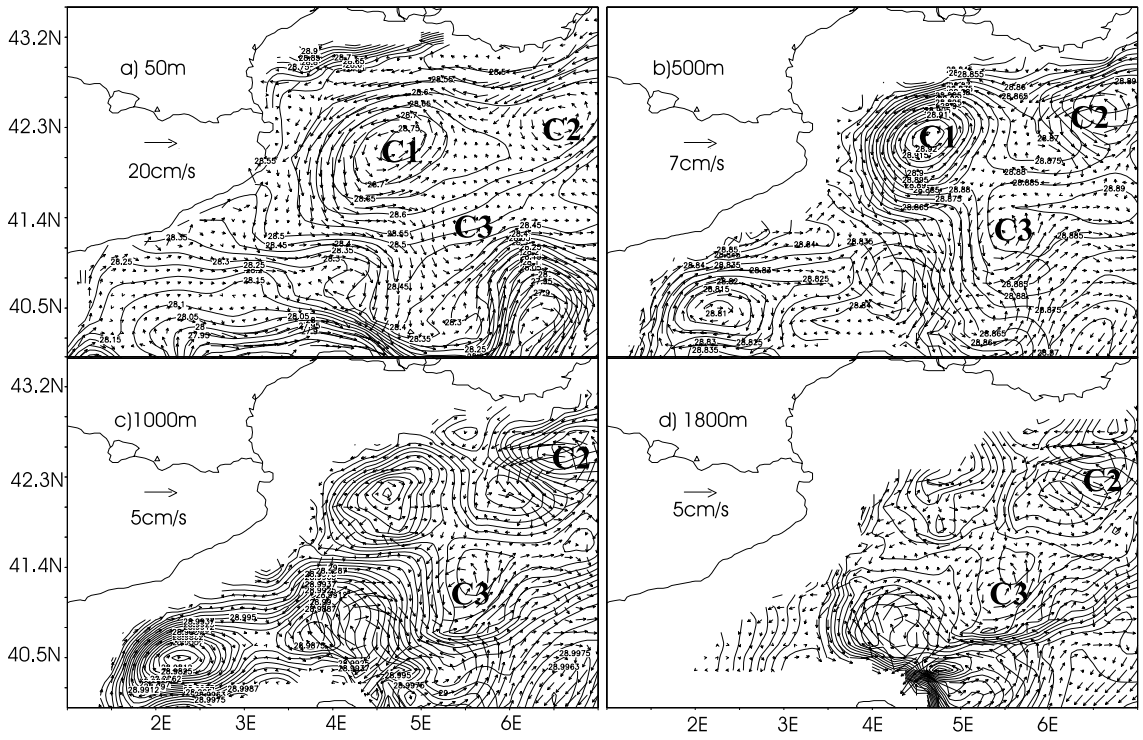


**Figure 4.** Mean velocity and density distributions in the Gulf of Lions for the period 1-3 January, 1992 at (a)50m; (b) 500m; (c) 1000m; (d) 1800m

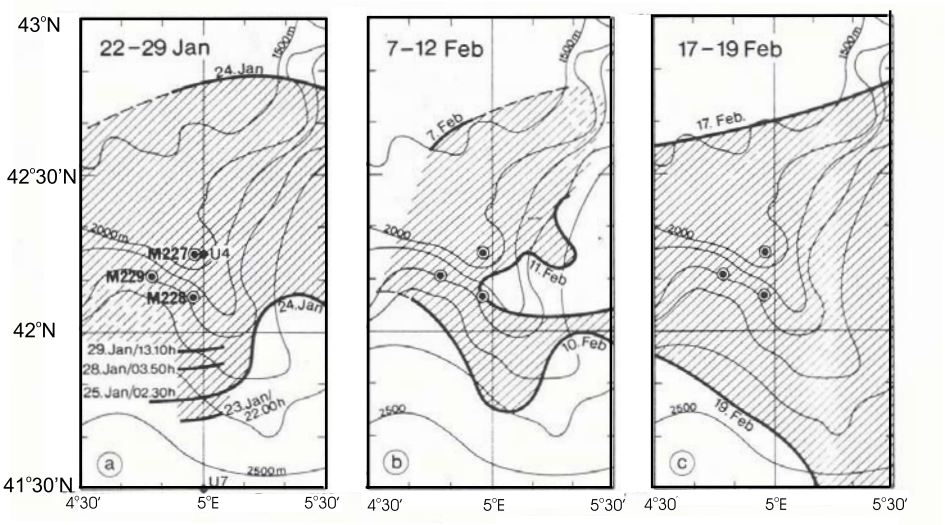


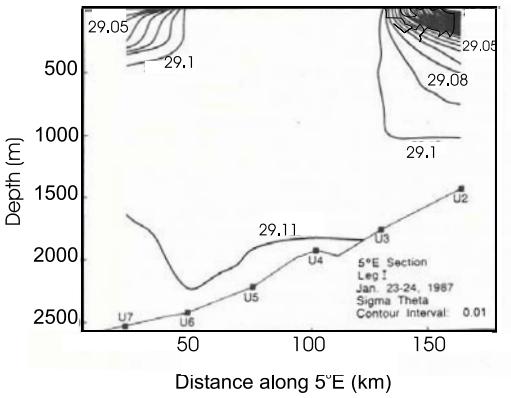


**Figure 5.** Horizontal and vertical extent of the mixed patch in 1987 (after Schott and Leaman, 1991, and Leaman and Schott, 1991). The horizontal extent is shown on upper panel for (a) 22-29 January, (b) 23-29 January, and (c) 17-23 February, 1987. The density cross section along 5$^o$E is shown on (d).

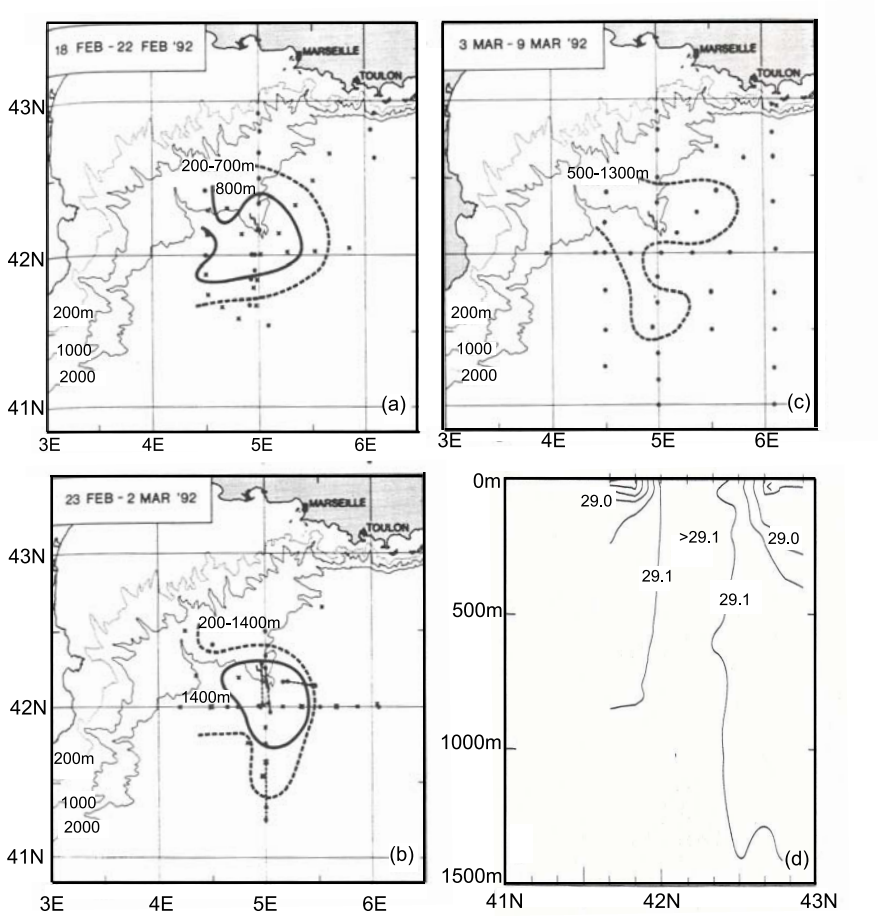


**Figure 6.** Horizontal and vertical extent of the deep convection area in 1992 (after Schott *et al.*, 1996). The horizontal extent and depths are plotted on the upper panel for (a) 18-22 February, 1992, (b) 23 February - 3 March, 1992, and (c) 3-9 March, 1992. The solid line indicates the horizontal boundaries of the surface convectively mixed layer. The numbers on the solid line show depth of the convection. The dashed line show the

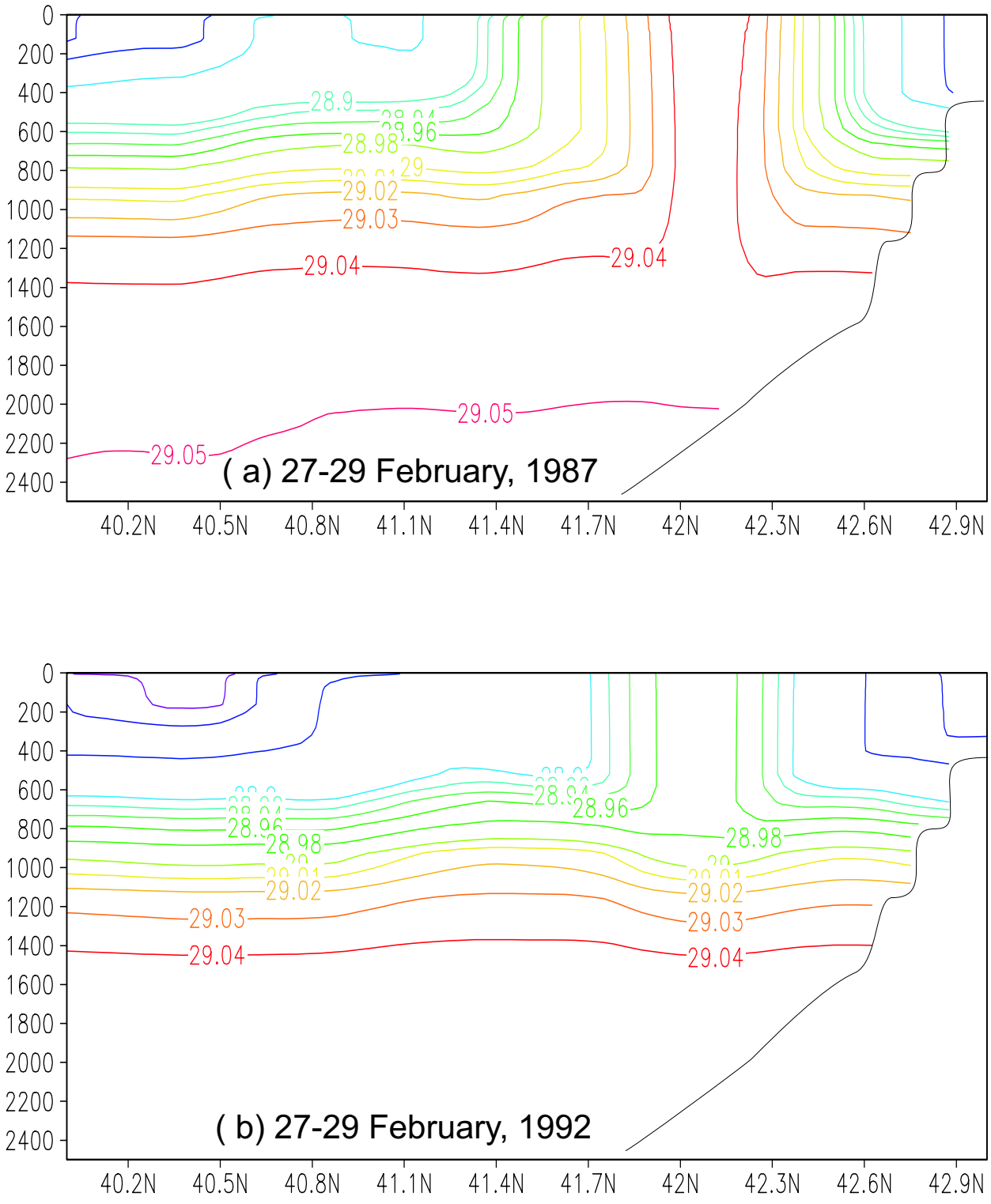





**Figure 7.** Vertical section of the density along the longitude 5$^o$E (a) 21-24 February, 1987; (b) 19-21 February, 1992

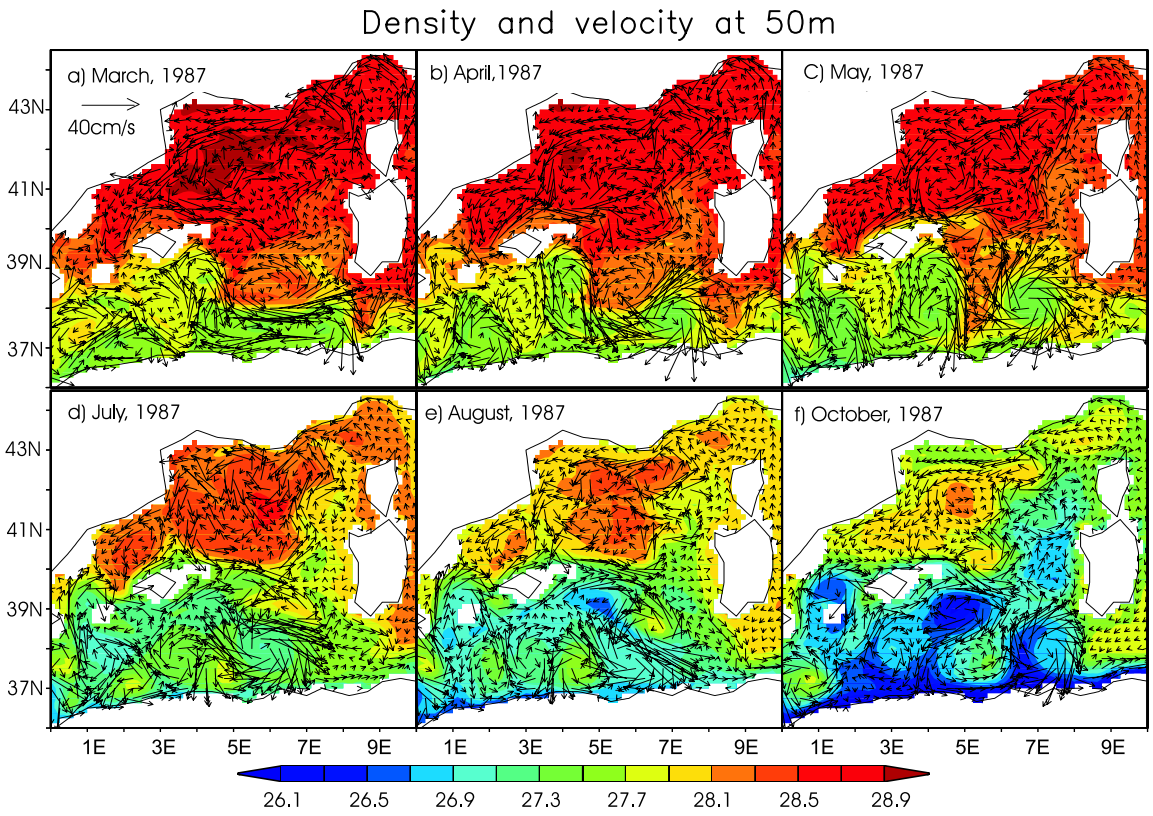


**Figure 8.** Monthly mean horizontal distribution of density and velocity fields at 50 m (a) March, 1987; (b) April, 1987; (c) May 1987; (d) June 1987; (e) August 1987; (f) October, 1987

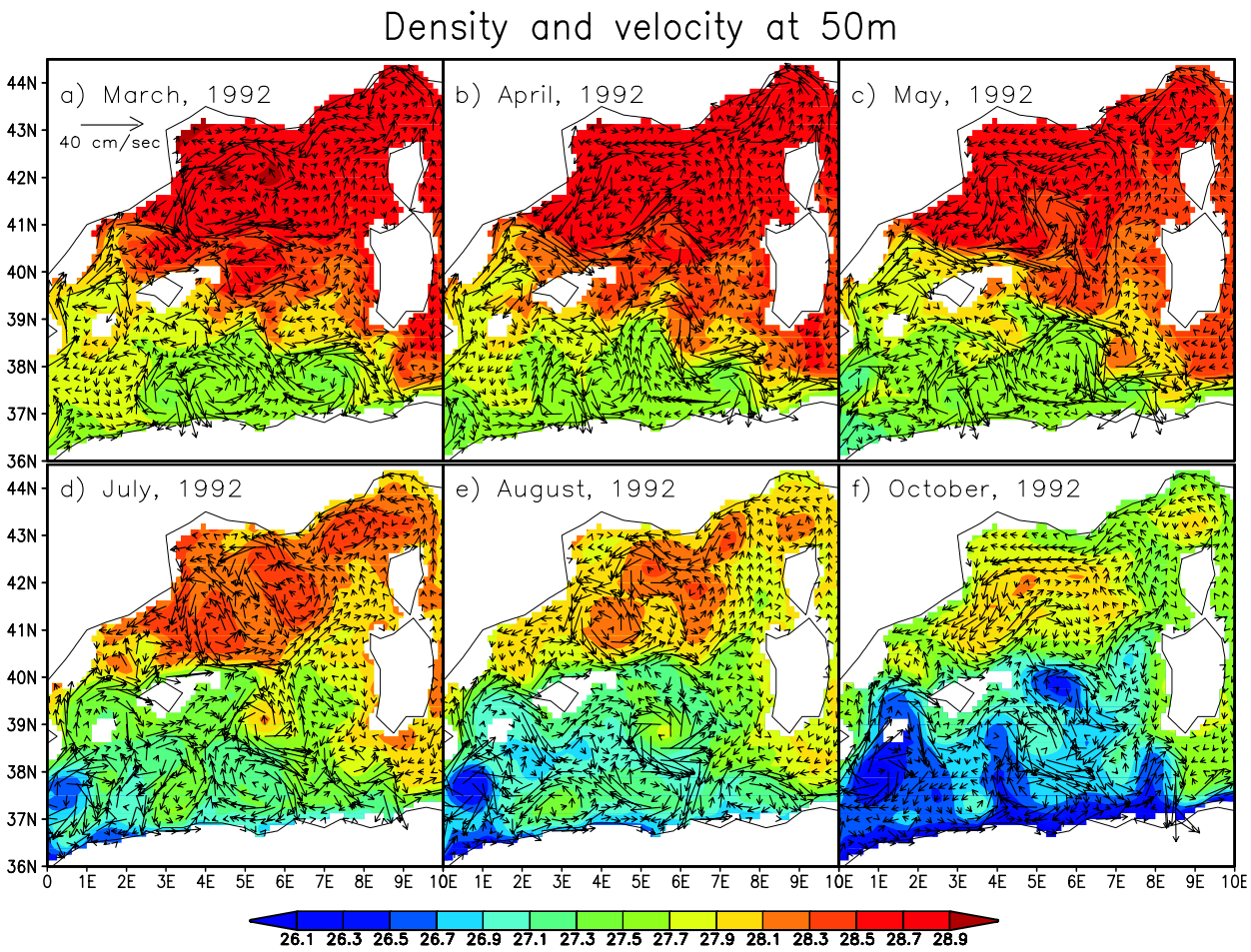


**Figure 9.** Monthly mean horizontal distribution of density and velocity fields at 50 m (a) March, 1992; (b) April, 1992; (c) May 1992; (d) June 1992; (e) August 1992; (f) October, 1992

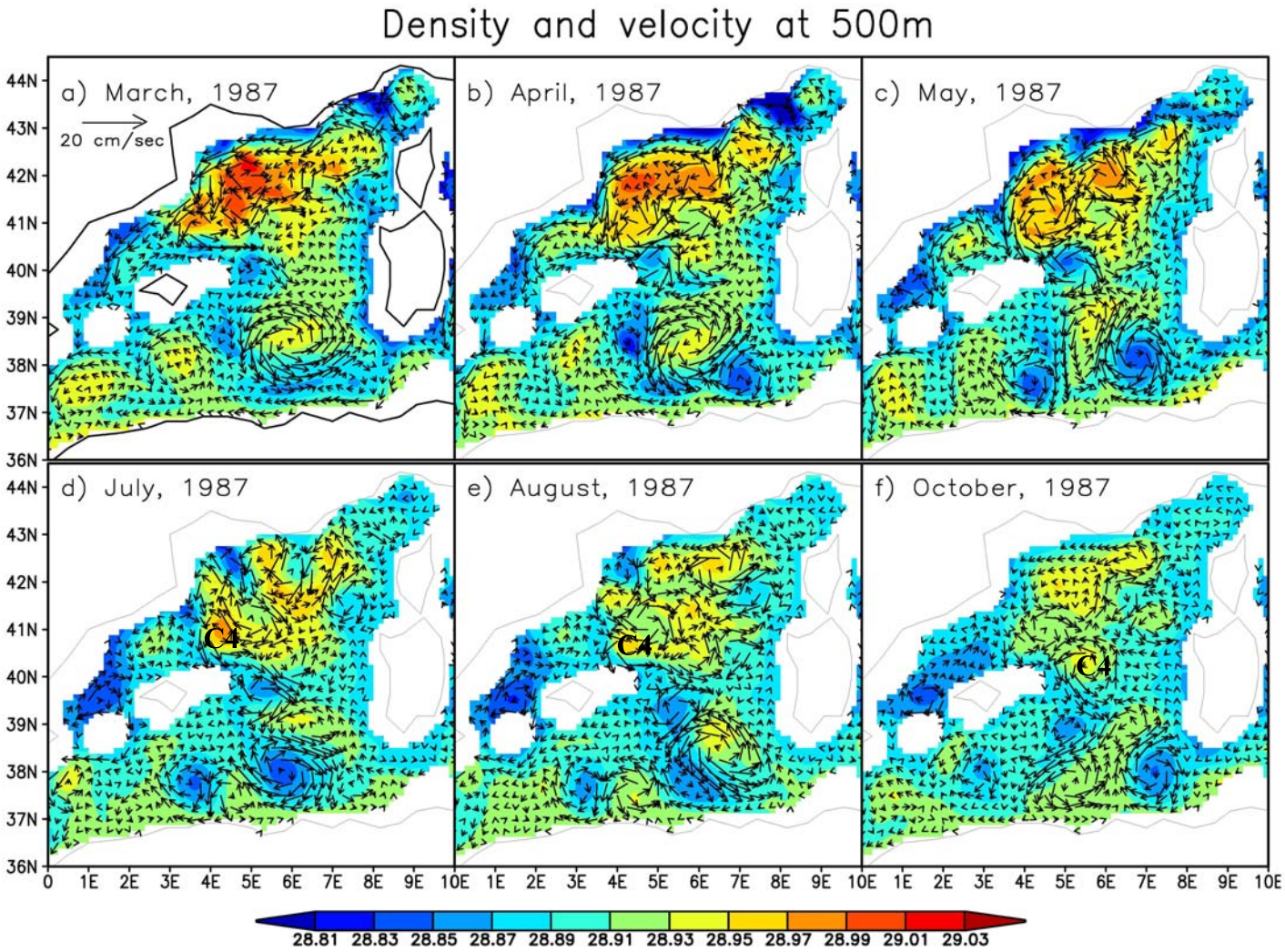


**Figure 10.** Monthly mean horizontal distribution of density and velocity fields at 500 m (a) March, 1987; (b) April, 1987; (c) May 1987; (d) June 1987; (e) August 1987; (f) October, 1987

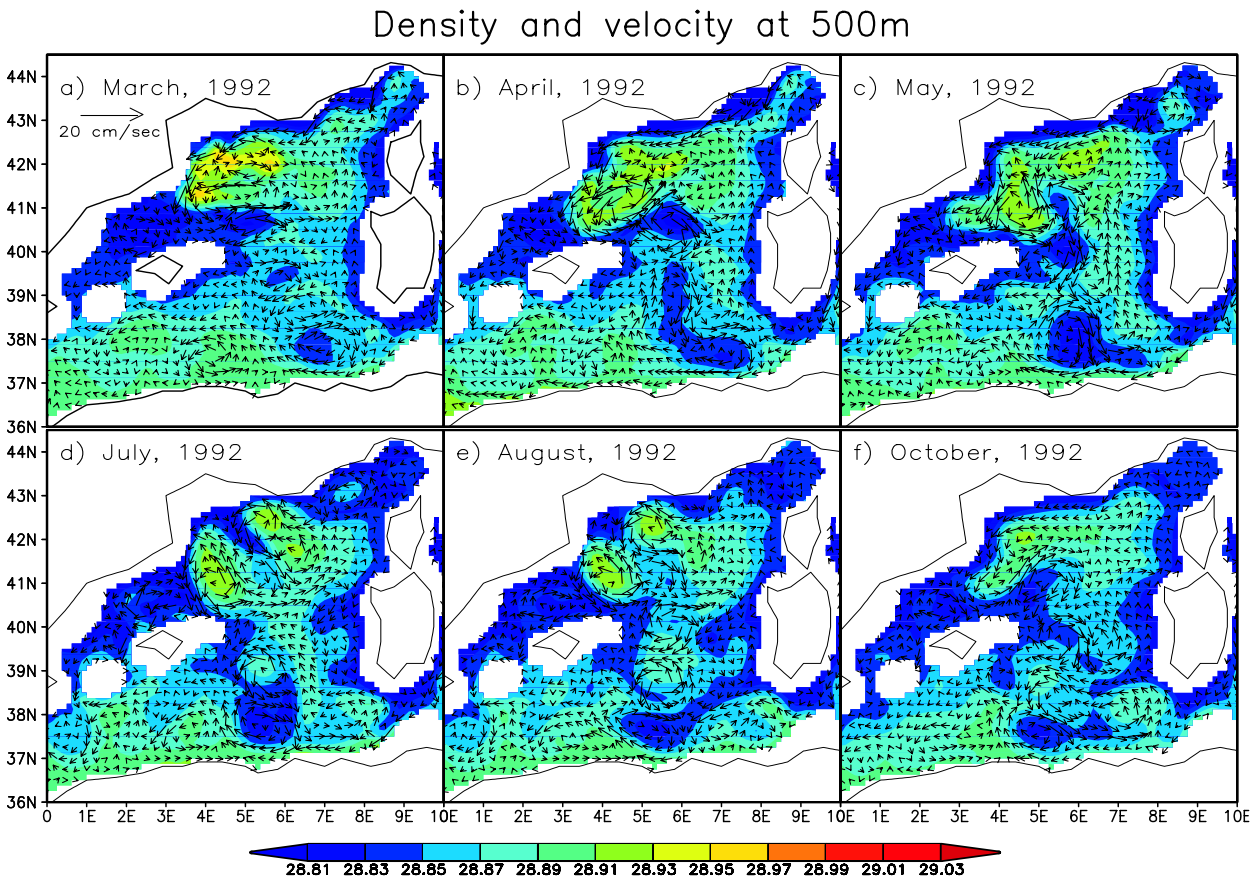


**Figure 11.** Monthly mean horizontal distribution of density and velocity fields at 500 m (a) March, 1992; (b) April, 1992; (c) May 1992; (d) June 1992; (e) August 1992; (f) October, 1992

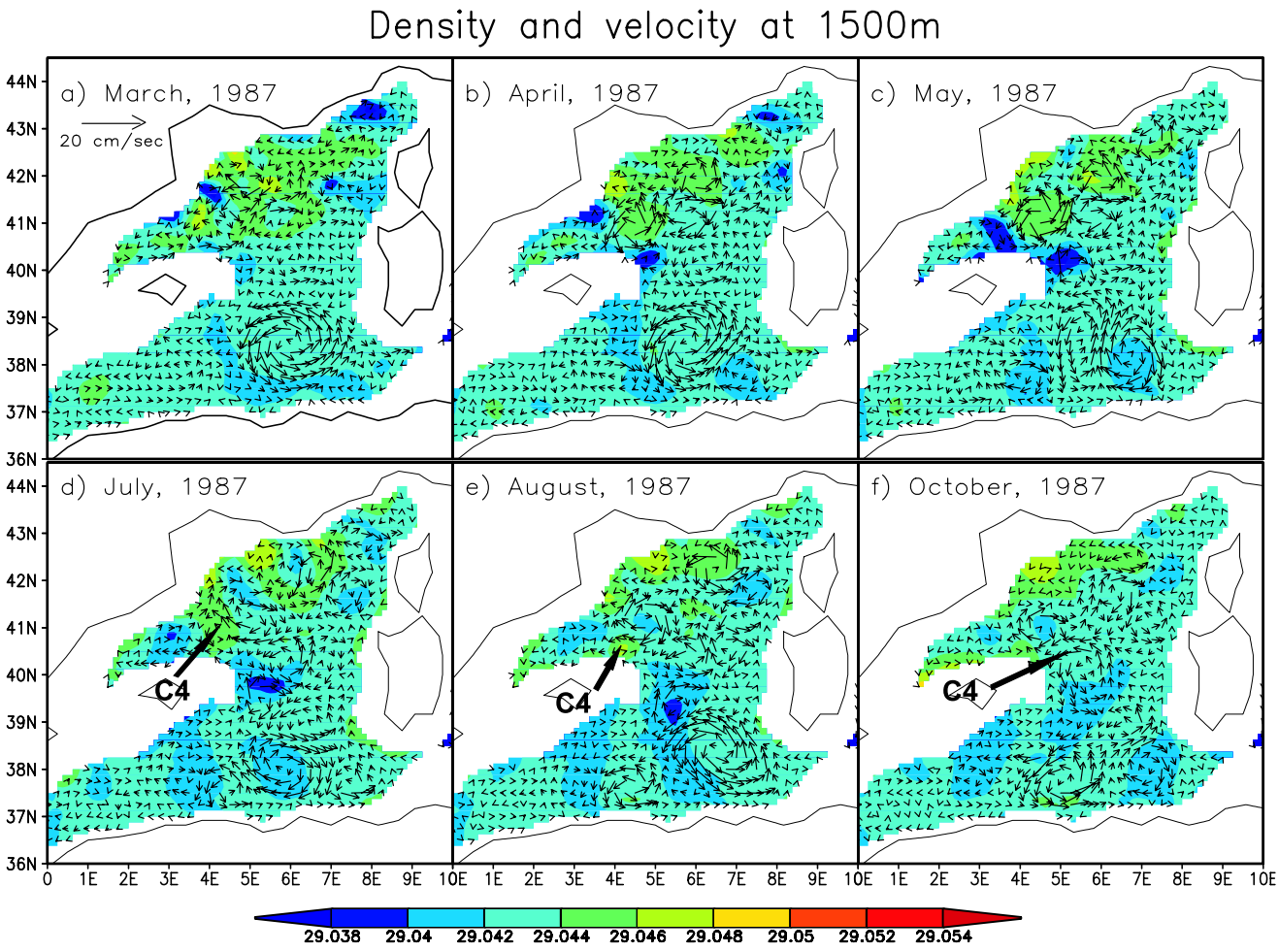


**Figure 12.** Monthly mean horizontal distribution of density and velocity fields at 1500 m (a) March, 1987; (b) April, 1987; (c) May 1987; (d) June 1987; (e) August 1987; (f) October, 1987

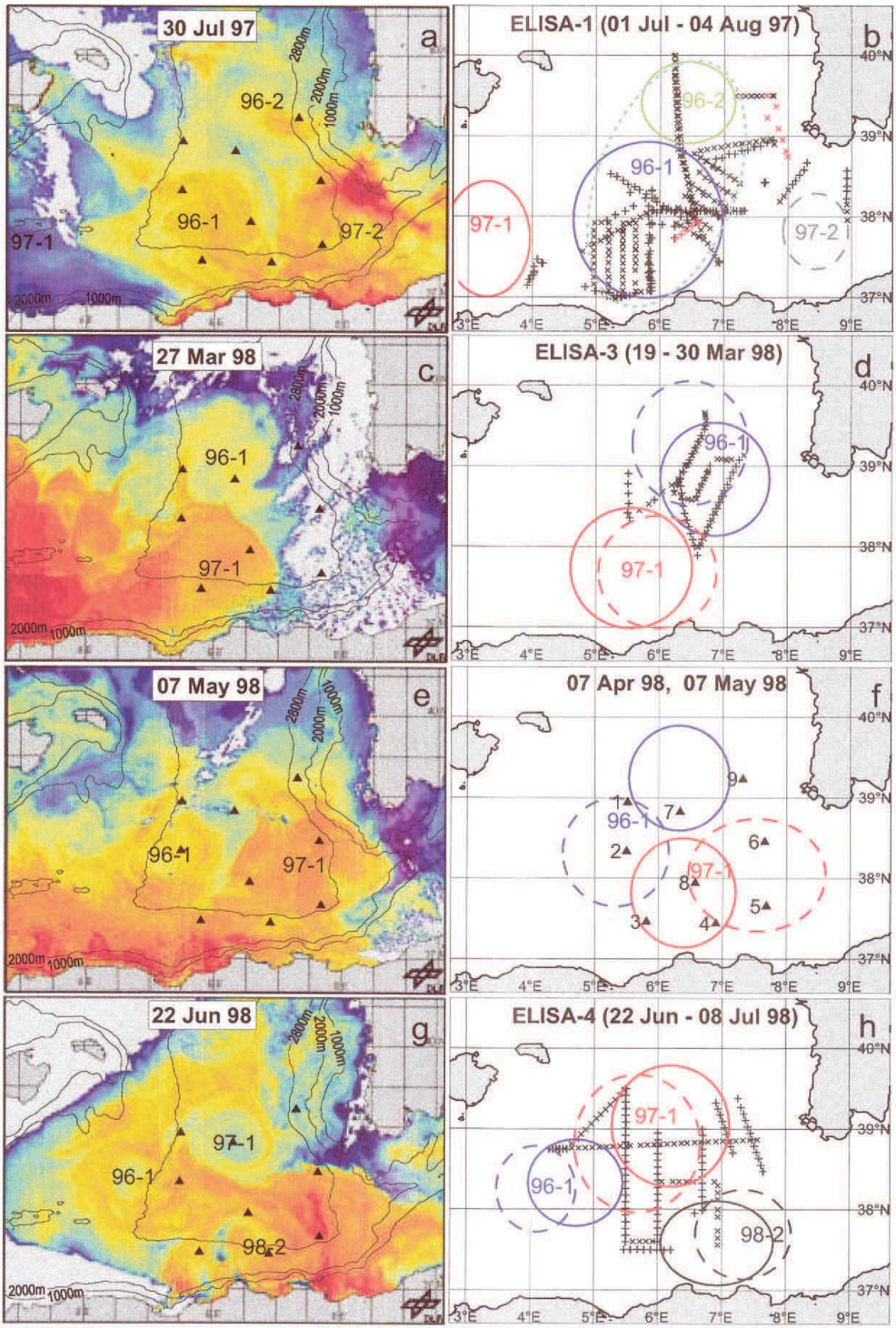




**Figure 13.** Synopsis of one-year ELISA experiment. a, c, e, g: NOAA-AVHRR infrared images. b,d,f,h scheme of the eddy field together with sampling moorings (Δ), CTD (+)

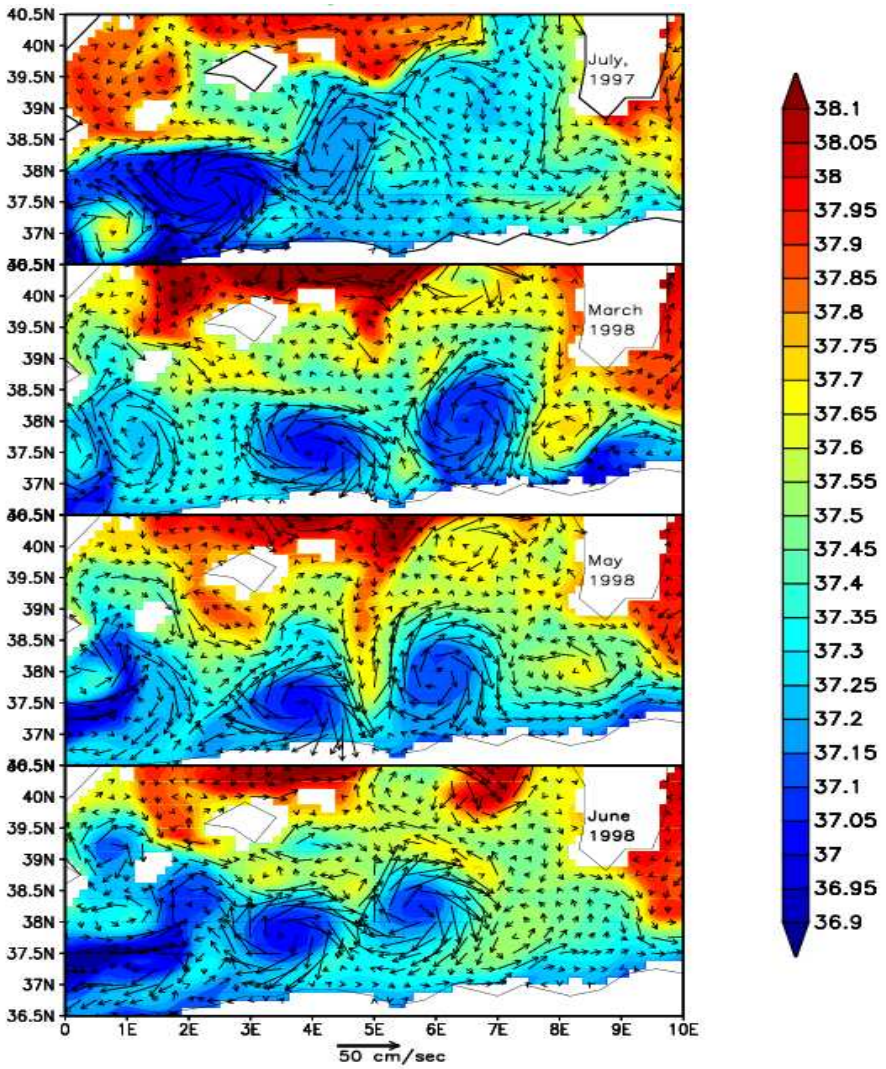


**Figure 14.** Horizontal distribution of temperature and velocity at 30m in the Algerian Basin in four different periods (a) 27 - 30, July, 1997 ; (b) 25-27 March, 1998; (c) 5-9 May, 1998; (d) 22 - 24 June, 1998.

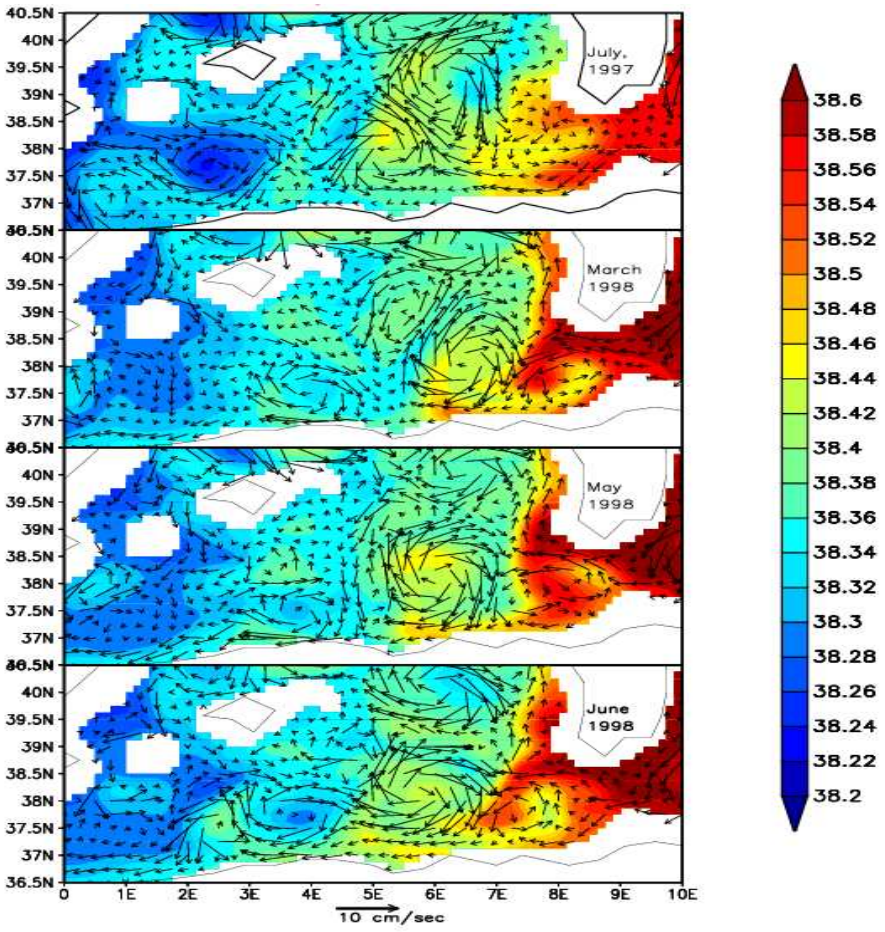


**Figure 15.** Horizontal distribution of salinity and velocity at 360 m in the Algerian Basin (a) 27 - 30, July, 1997; (b) 25-27 March, 1998; (c) 5-9 May, 1998; (d) 22 - 24 June, 1998.

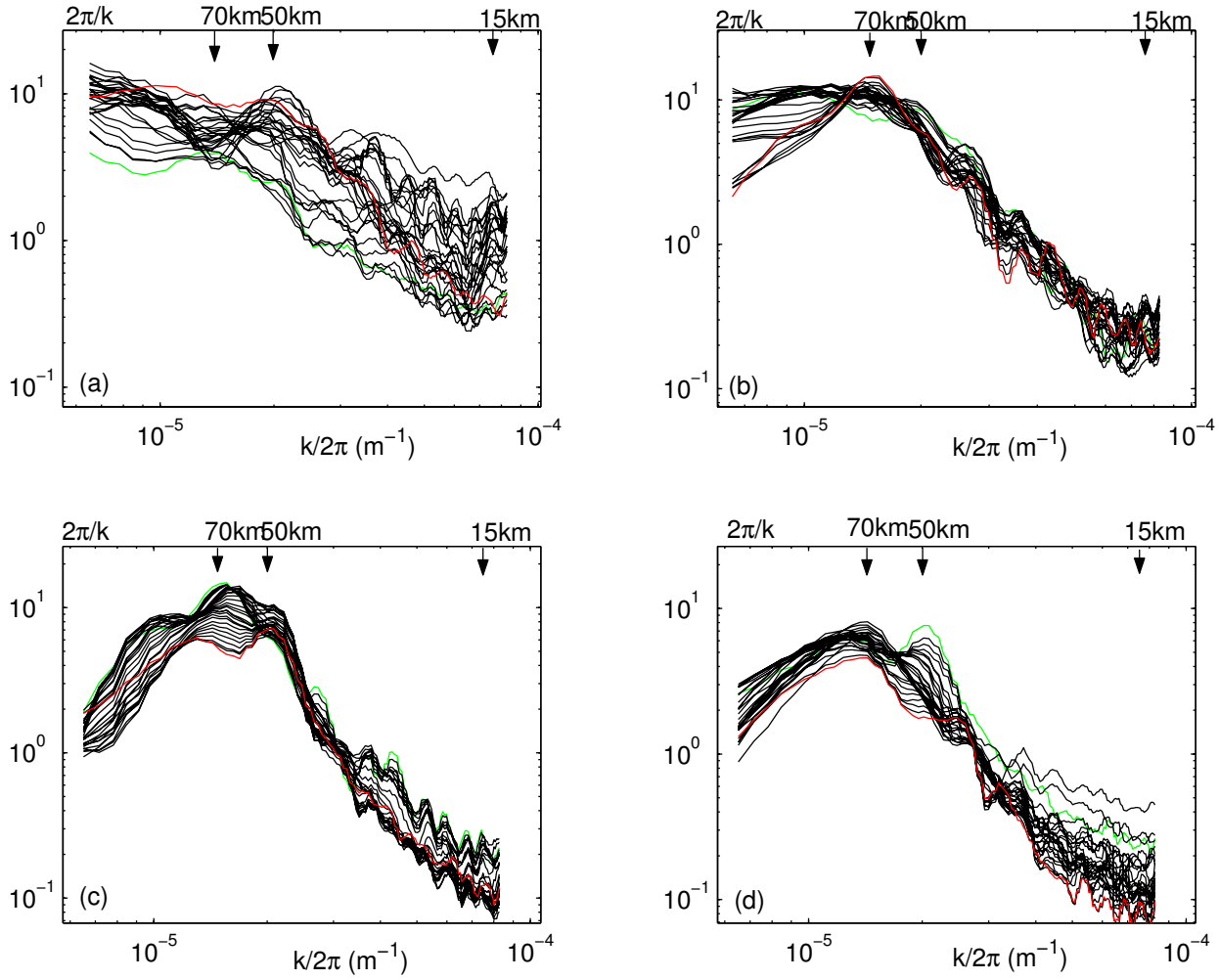


**Figure 16.** 3-days mean barotropic kinetic energy spectra curves of the barotropic flow in the Gulf of Lions for (a) winter, (b) spring, (c) summer and (d) autumn. The green curve shows the spectra at the beginning of each period, the red line - the spectra at the end of the period.

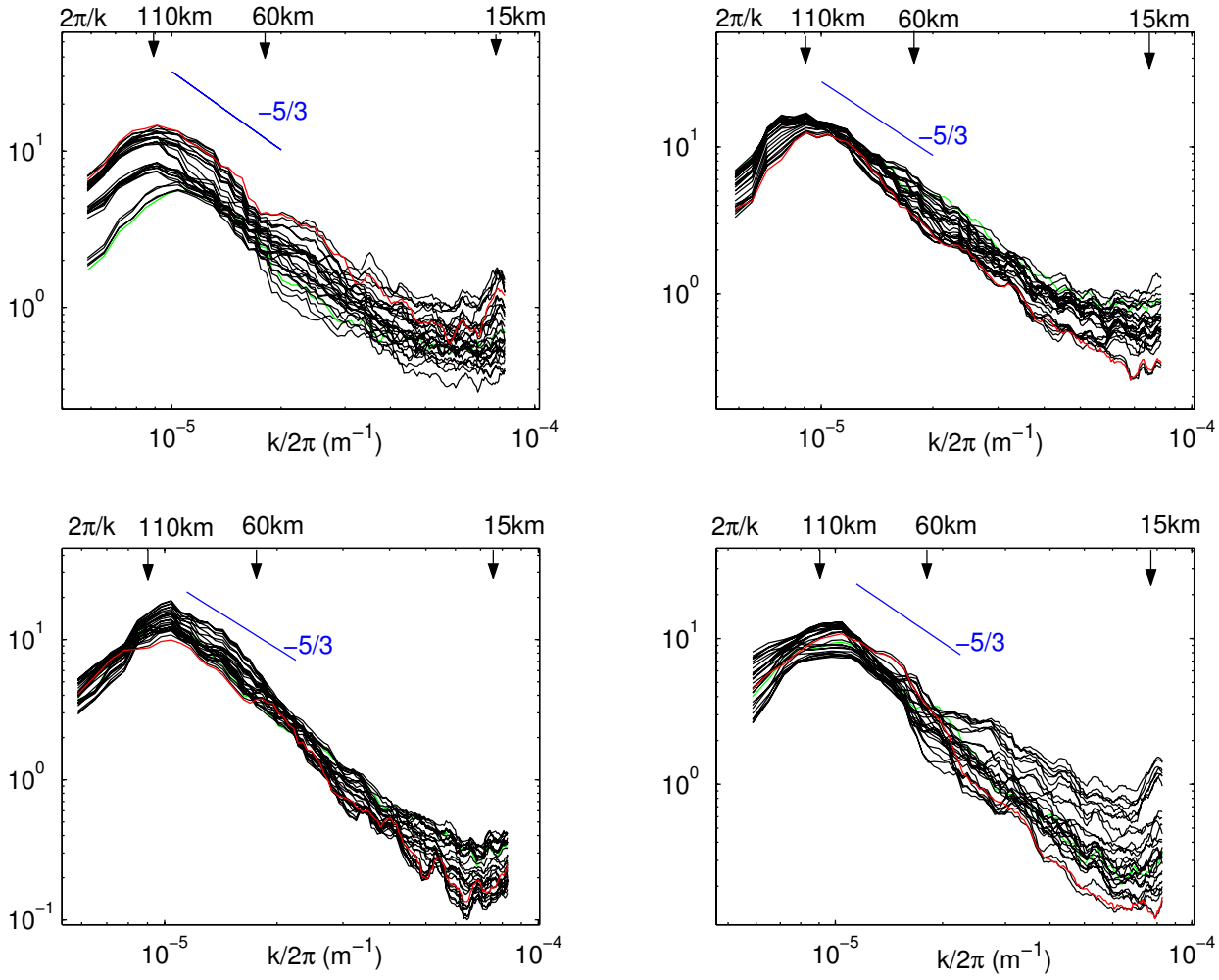


**Figure 17.** 3-days mean barotropic kinetic energy spectra curves of the barotropic flow in the Algerian Basin for (a) winter, (b) spring, (c) summer and (d) autumn. The green curve shows the spectra at the beginning of each period, the red line - the spectra at the end of the period.

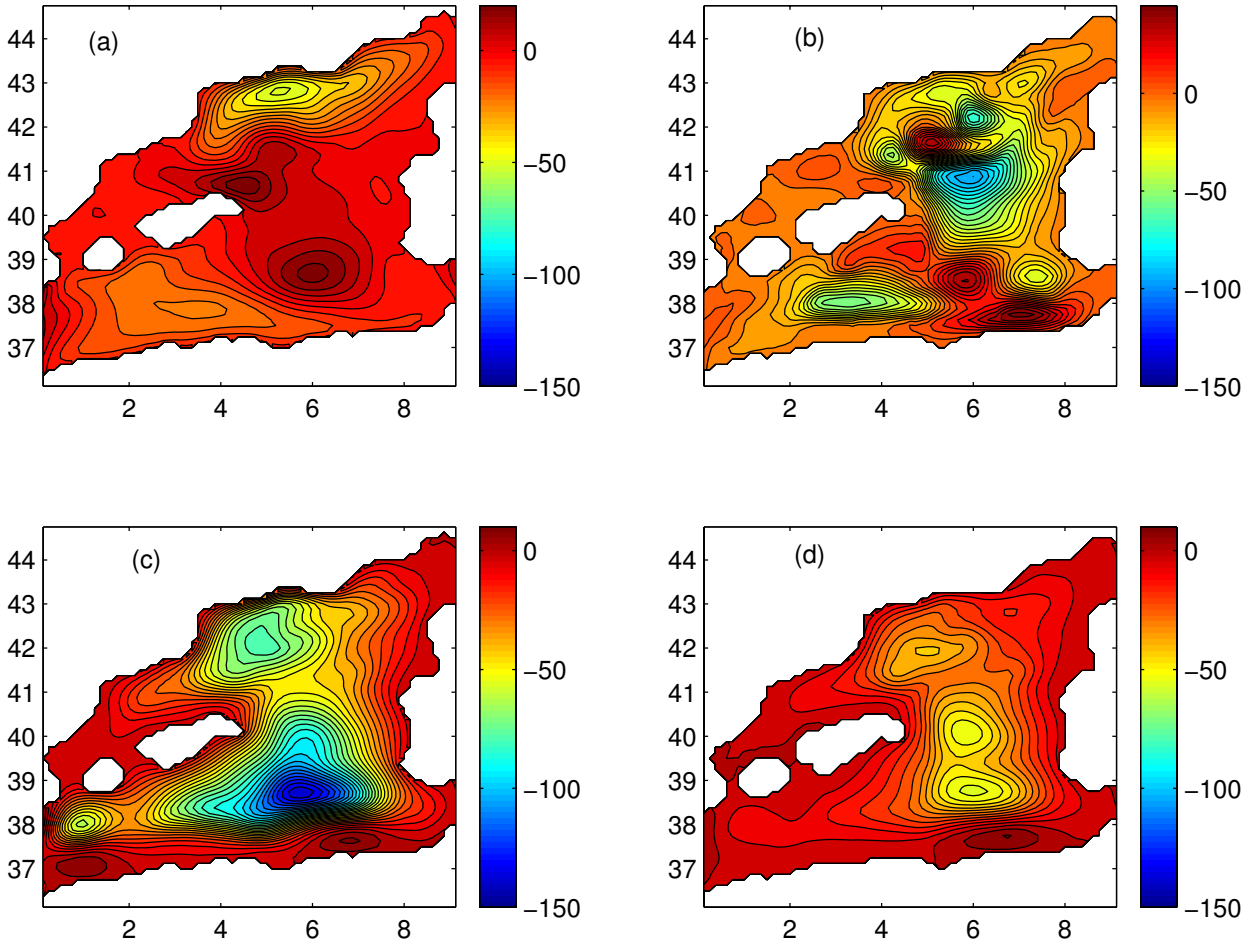


**Figure 18.** Stream function (Sv kg/$m^3$) of the (a) mean transport in the intermediate layer; (b) mean transport in the deep layer; (c) eddy-induced transport in the intermediate layer; and (d) eddy-induced transport in the deep layer.

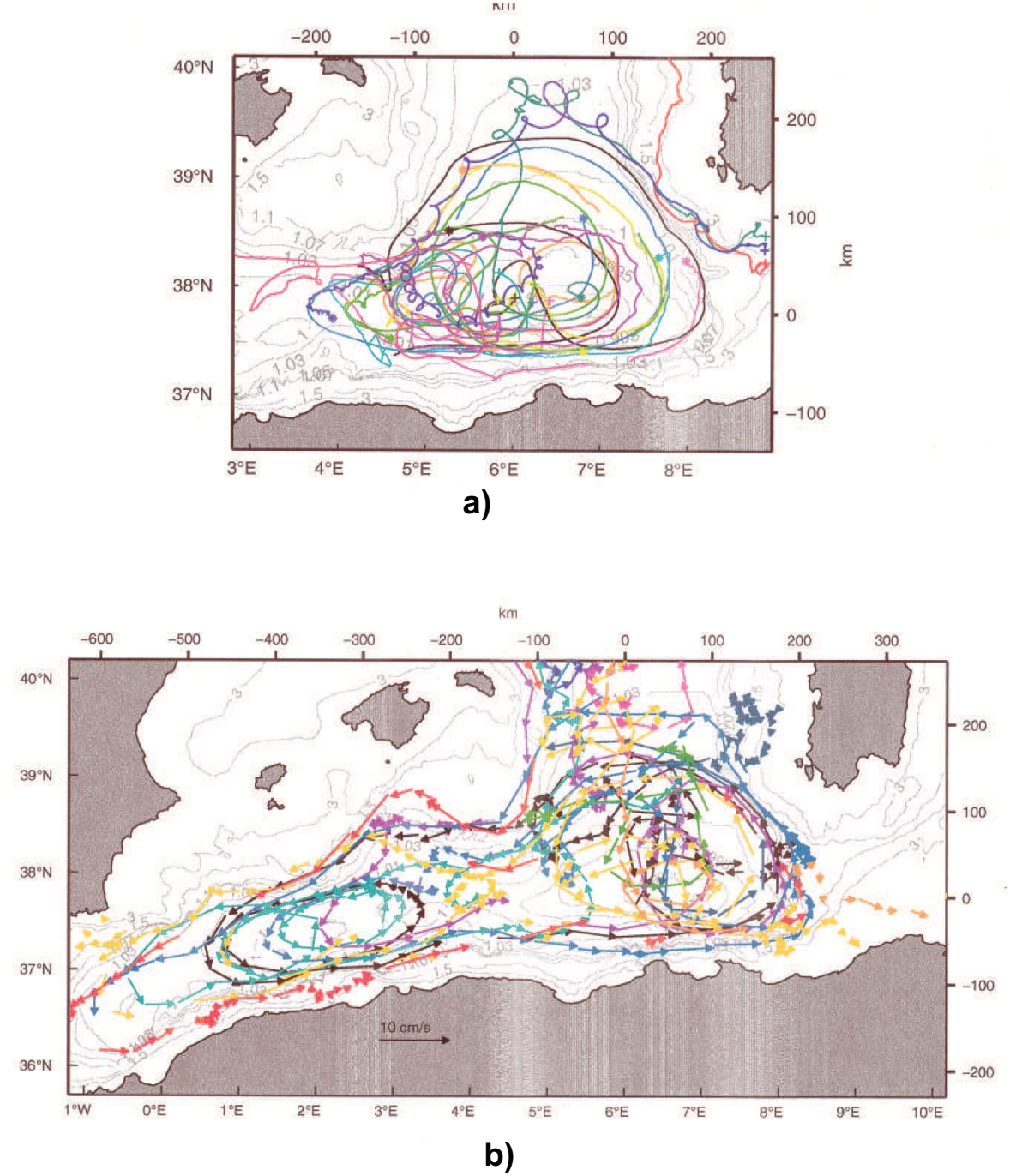


**Figure 19.** (a) Trajectories of the RAFOS floats at 600 m from July 14, 1997 until June 24, 1998. superimposed on f/H contours. (b) Trajectories of profiling floats drifting at 1200 and 2000. Arrows indicate the drift at depth during 8 days. One color of each float. (after Testor *et al.*, 2005)

**Table 1.** Components of energy balance in the surface layer of Gulf of Lions

| *Parameter* | Winter | Spring | Summer | Autumn |
|---|---|---|---|---|
| $KE_m[J/m^3]$ | 2.77 | 3.40 | 2.13 | 1.87 |
| $KE_e[J/m^3]$ | 2.63 | 4.54 | 3.80 | 3.83 |
| $APE_m[J/m^3]$ | 674.79 | 85.09 | 27.89 | 23.69 |
| $APE_e[J/m^3]$ | 853.06 | 17.99 | 12.41 | 26.35 |
| $T_1[10^{-7}W/m^3]$ | -318.67 | -41.36 | -16.7 | -14.42 |
| $T_2[10^{-7}W/m^3]$ | -4.02 | -3.39 | -6.15 | -4.55 |

**Table 2.** Components of energy balance in the intermediate layer of Gulf of Lions

| *Parameter* | Winter | Spring | Summer | Autumn |
|---|---|---|---|---|
| $KE_m[J/m^3]$ | 0.45 | 0.93 | 0.40 | 0.29 |
| $KE_e[J/m^3]$ | 0.77 | 1.58 | 1.11 | 0.81 |
| $APE_m[J/m^3]$ | 31.13 | 26.53 | 28.59 | 32.35 |
| $APE_e[J/m^3]$ | 7.91 | 7.29 | 8.00 | 7.14 |
| $T_1[10^{-7}W/m^3]$ | -14.05 | -19.86 | -11.66 | -4.33 |
| $T_2[10^{-7}W/m^3]$ | -0.33 | -0.55 | -0.42 | -0.35 |

**Table 3.** Components of energy balance in the deep layer of Gulf of Lions

| *Parameter* | Winter | Spring | Summer | Autumn |
|---|---|---|---|---|
| $KE_m[J/m^3]$ | 0.09 | 0.19 | 0.08 | 0.05 |
| $KE_e[J/m^3]$ | 0.37 | 0.83 | 0.52 | 0.42 |
| $APE_m[J/m^3]$ | 831.29 | 815.26 | 819.15 | 829.20 |
| $APE_e[J/m^3]$ | 1.93 | 2.24 | 1.92 | 1.74 |
| $T_1[10^{-7}W/m^3]$ | -1.09 | -2.39 | -0.81 | -0.51 |
| $T_2[10^{-7}W/m^3]$ | 0.13 | 0.07 | -0.05 | 0.04 |

**Table 4.** Components of energy balance in the surface layer of the Algerian Basin

| *Parameter* | Winter | Spring | Summer | Autumn |
|---|---|---|---|---|
| $KE_m[J/m^3]$ | 1.89 | 2.07 | 2.22 | 1.36 |
| $KE_e[J/m^3]$ | 10.17 | 12.56 | 11.52 | 8.43 |
| $APE_m[J/m^3]$ | 3860.73 | 613.74 | 221.03 | 136.82 |
| $APE_e[J/m^3]$ | 950.43 | 129.21 | 73.90 | 63.97 |
| $T_1[10^{-7}W/m^3]$ | -1251.78 | -174.70 | -10.63 | -41.65 |
| $T_2[10^{-7}W/m^3]$ | -9.49 | -4.31 | 5.95 | -11.59 |

**Table 5.** Components of energy balance in the intermediate layer of the Algerian Basin

| *Parameter* | Winter | Spring | Summer | Autumn |
|---|---|---|---|---|
| $KE_m[J/m^3]$ | 0.12 | 0.15 | 0.21 | 0.13 |
| $KE_e[J/m^3]$ | 1.12 | 1.40 | 1.40 | 1.07 |
| $APE_m[J/m^3]$ | 69.29 | 71.00 | 69.43 | 65.50 |
| $APE_e[J/m^3]$ | 10.45 | 12.03 | 10.71 | 9.13 |
| $T_1[10^{-7}W/m^3]$ | -1.58 | -1.26 | -0.67 | -0.57 |
| $T_2[10^{-7}W/m^3]$ | -0.20 | -0.32 | 0.23 | -0.21 |

**Table 6.** Components of energy balance in the deep layer of the Algerian basin

| *Parameter* | Winter | Spring | Summer | Autumn |
|---|---|---|---|---|
| $KE_m[J/m^3]$ | 0.03 | 0.04 | 0.11 | 0.11 |
| $KE_e[J/m^3]$ | 0.63 | 0.74 | 0.75 | 0.61 |
| $APE_m[J/m^3]$ | 896.99 | 893.47 | 882.94 | 885.75 |
| $APE_e[J/m^3]$ | 1.26 | 1.33 | 1.30 | 1.28 |
| $T_1[10^{-7}W/m^3]$ | -0.10 | -0.07 | -0.03 | -0.05 |
| $T_2[10^{-7}W/m^3]$ | -0.00 | -0.09 | 0.10 | -0.13 |